

Gaussian orthogonal latent factor processes for large incomplete matrices of correlated data

Mengyang Gu* and Hanmo Li†

Abstract

We introduce Gaussian orthogonal latent factor processes for modeling and predicting large correlated data. To handle the computational challenge, we first decompose the likelihood function of the Gaussian random field with a multi-dimensional input domain into a product of densities at the orthogonal components with lower-dimensional inputs. The continuous-time Kalman filter is implemented to compute the likelihood function efficiently without making approximations. We also show that the posterior distribution of the factor processes is independent, as a consequence of prior independence of factor processes and orthogonal factor loading matrix. For studies with large sample sizes, we propose a flexible way to model the mean, and we derive the marginal posterior distribution to solve identifiability issues in sampling these parameters. Both simulated and real data applications confirm the outstanding performance of this method.

Keywords— Orthogonality, marginalization, correlated data, Gaussian processes

1 Introduction

Large spatial, spatio-temporal, and functional data are commonly used in various studies, including geological hazard quantification, engineering, and medical imaging, to facilitate scientific discoveries. Many data sets are observed on incomplete matrices with missing values due to the limitation of the technique or computational cost.

Gaussian processes (GPs) are widely used for modeling correlated data (Banerjee et al., 2014; Cressie and Cassie, 1993). Computing the likelihood function from a GP model, however, generally takes $O(N_o^3)$ operations in finding the inverse and determinant of the covariance matrix, where N_o is the number of observations. The computational bottleneck prevents modeling a large correlated data set by GPs directly. Tremendous efforts have been made to approximate a GP model in recent studies, including, for example, stochastic

*Department of Statistics and Applied Probability, University of California, Santa Barbara, CA, Email: mengyang@pstat.ucsb.edu

†Department of Statistics and Applied Probability, University of California, Santa Barbara, CA 93106, USA, Email: hanmo@pstat.ucsb.edu

partial differential equation approach (Lindgren et al., 2011; Rue et al., 2009), hierarchical nearest neighbor methods (Datta et al., 2016), multi-resolution process (Katzfuss, 2017), local Gaussian process approach (Gramacy and Apley, 2015), periodic embedding (Guinness and Fuentes, 2017; Stroud et al., 2017) and covariance tapering (Kaufman et al., 2008), which have obtained wide attention in recent years.

Compared to a large number of studies on approximating GPs, less progress have been made on efficiently computing the likelihood function without approximation. In this work, we propose a flexible and computationally feasible approach to model large incomplete matrix observations of correlated data, called Gaussian orthogonal latent factor (GOLF) processes. Bayesian inference was derived to assess the uncertainty in parameter estimation and predictions. GPs with product covariance functions on lattice observations or semiparametric latent factor models (Sacks et al., 1989; Kennedy and O’Hagan, 2001; Teh et al., 2005) can be represented as full-rank GOLF processes, which permit much smaller computational costs than directly computing the likelihood function and making predictions. Further reducing the computational cost can be achieved by low-rank GOLF processes, where the computational cost is similar to the order of principal component analysis.

We highlight a few contributions of this work. We first show that for GPs with product covariance functions or semiparametric latent factor models, if the latent factor loading matrix is orthogonal, prior independence of latent factor processes implies posterior independence of factor processes. The new finding allows one to decompose the likelihood function of lattice data into a product of densities of projected output, which greatly reduces the computational complexity. Separate continuous-time Kalman filters can be applied to compute the posterior distributions of factor processes at lower dimensional inputs in parallel, which has linear computational operations with respect to the number of observations. Second, as a large number of observations provide rich information, we introduce a flexible way to model the mean function and derive the marginal posterior distribution of the linear coefficients, to solve identifiability issues in posterior sampling. Furthermore, compared with the maximum marginal likelihood estimation of factor loadings derived in Gu and Shen (2020), our approach is applicable to model observations on incomplete lattice. Finally, we developed Bayesian inference for uncertainty assessment, which is critically important for inverse problems in applications (Kennedy and O’Hagan, 2001; Bayarri et al., 2007).

The purpose of this work are twofold. First, we aim to develop a pipeline of computationally efficient methods of modeling correlated data with multi-dimensional input without approximating the likelihood function. Properties of GOLF processes derived in this work are useful for developing an efficient approximation algorithm for scenarios with multi-dimensional input variables. Besides, the nonseparable covariance and coordinate-specific mean coefficients proposed in this work provide flexible choices for models of local information. Second, we primarily focus on applications based on images, which include inverse problems by satellite radar interferograms (Anderson et al., 2019), and estimating dynamic information from microscopic videos (Cerbino and Trappe, 2008). Our approach allows for efficient Bayesian inference in a large sample scenario.

The rest of the article is organized as follows. In Section 2.1, we introduce the GOLF model with an emphasis on the orthogonal decomposition of the likelihood function and posterior independence of latent factor processes. The flexible mean function, spatial latent factor loading matrix and kernel functions are discussed in Section 2.2-2.4, respectively.

We introduce the Markov Chain Monte Carlo (MCMC) algorithm and discuss the computational complexity in Section 3.1. In Section 3.2, we introduce the continuous-time Kalman filter in computing the likelihood function with linear computational complexity. Section 4 compares our approach with other alternatives, and numerical results for comparing these approaches are presented in Section 5-6. We conclude this work and discuss several potential extensions in Section 7. Proofs of lemmas and theorems are given in supplementary materials. The data and code used in this paper are publicly available (<https://github.com/UncertaintyQuantification/GOLF>).

2 Gaussian orthogonal latent factor processes

2.1 Orthogonal decomposition and posterior independence

Let $\mathbf{y}_s(\mathbf{x}) = (y_{s_1}(\mathbf{x}), \dots, y_{s_{n_1}}(\mathbf{x}))^T$ be an $n_1 \times 1$ vector of observations at coordinates $\mathbf{s} = (\mathbf{s}_1, \dots, \mathbf{s}_{n_1})^T$ with $\mathbf{s}_i \in \mathbb{R}^{p_1}$ for $i = 1, \dots, n_1$ and input $\mathbf{x} \in \mathbb{R}^{p_2}$. For spatially correlated data, for instance, s and x denote the latitude and longitude, respectively, and in spatio-temporal models, the spatial coordinates and time points can be defined as \mathbf{s} and x , respectively.

Consider the latent factor model:

$$\mathbf{y}_s(\mathbf{x}) = \mathbf{m}_s(\mathbf{x}) + \mathbf{A}_s \mathbf{z}(\mathbf{x}) + \boldsymbol{\epsilon}, \quad (1)$$

where $\mathbf{A}_s = [\mathbf{a}_1, \dots, \mathbf{a}_d]$ is a $n_1 \times d$ factor loading matrix and $\mathbf{z}(\mathbf{x}) = (z_1(\mathbf{x}), \dots, z_d(\mathbf{x}))^T$ is a d -dimensional factor processes with $d \leq n_1$, $\boldsymbol{\epsilon} \sim \mathcal{N}(0, \sigma_0^2 \mathbf{I}_{n_1})$ being independent Gaussian noises. The mean function $\mathbf{m}_s(\mathbf{x}) = (m_{s_1}(\mathbf{x}), \dots, m_{s_{n_1}}(\mathbf{x}))^T$ is typically modeled via a linear trend of regressors, which will be discussed in Section 2.2.

As data are typically positively correlated at two nearby inputs, we assume $z_l(\cdot)$ independently follows a zero-mean Gaussian process (GP), meaning that for any $\{\mathbf{x}_1, \dots, \mathbf{x}_{n_2}\}$, $\mathbf{Z}_l^T = (Z_l(\mathbf{x}_1), \dots, Z_l(\mathbf{x}_{n_2}))^T$ is a multivariate normal distribution:

$$(\mathbf{Z}_l^T \mid \Sigma_l) \sim \mathcal{N}(\mathbf{0}, \Sigma_l) \quad (2)$$

where the (i, j) th entry of the covariance matrix is $\sigma_l^2 K_l(\mathbf{x}_i, \mathbf{x}_j)$ with kernel function $K_l(\cdot, \cdot)$ and variance parameter σ_l^2 , for $l = 1, \dots, d$. Here we assume independence between the factor processes *a priori*. A detailed comparison between our approach and other related approaches is discussed in Section 4.

Note that only the d -dimensional linear subspace of factor loadings \mathbf{A}_s can be identified if not further specification of factor loading matrix \mathbf{A}_s is made, as the model (1) is unchanged if the pair $(\mathbf{A}_s, \mathbf{z}(\mathbf{x}))$ is replaced by $(\mathbf{A}_s \mathbf{G}, \mathbf{G}^{-1} \mathbf{z}(\mathbf{x}))$ for any invertible matrix \mathbf{G} . Besides, the computation could be challenging when the number of factors or input parameters is large. Thus, we assume that the column of \mathbf{A}_s is orthonormal.

Assumption 1.

$$\mathbf{A}_s^T \mathbf{A}_s = \mathbf{I}_d. \quad (3)$$

Assumption (1) may be replaced by $\mathbf{A}_s^T \mathbf{A}_s = \mathbf{\Lambda}$, where $\mathbf{\Lambda}$ is a diagonal matrix. Since we estimate variance parameters $\boldsymbol{\sigma}^2 = (\sigma_1^2, \dots, \sigma_d^2)^T$ of latent factor processes by data, diagonal terms of $\mathbf{\Lambda}$ are redundant. Thus we proceed with the Assumption 1.

Let us first assume we have an $n_1 \times n_2$ matrix of observations $\mathbf{Y} = [\mathbf{y}_s(\mathbf{x}_1), \dots, \mathbf{y}_s(\mathbf{x}_{n_2})]$ at inputs $\{\mathbf{x}_1, \dots, \mathbf{x}_{n_2}\}$, and then we extend our method to incomplete matrix observations in the Section 3. Denote \mathbf{B} the regression parameters in the $n_1 \times n_2$ mean matrix $\mathbf{M} = (\mathbf{m}_s(\mathbf{x}_1), \dots, \mathbf{m}_s(\mathbf{x}_{n_2}))$. Denote $\boldsymbol{\Theta} = (\mathbf{A}_s, \mathbf{B}, \boldsymbol{\sigma}^2, \boldsymbol{\gamma})$, which contains the factor loadings, mean parameters, variance parameters and range parameters in the kernel functions. Further let $\mathbf{A}_F = [\mathbf{A}_s, \mathbf{A}_c] = [\mathbf{a}_1, \mathbf{a}_2, \dots, \mathbf{a}_{n_1}]$, where \mathbf{A}_c is an $n_1 \times (n_1 - d)$ matrix of the orthogonal complement of \mathbf{A}_s . Assumption 1 allows us to decompose the marginal likelihood (after integrating out the random factor \mathbf{Z}) into a product of multivariate normal densities of the outcomes at the projected coordinates:

$$p(\mathbf{Y} \mid \boldsymbol{\Theta}) = \prod_{l=1}^d \mathcal{PN}(\tilde{\mathbf{y}}_l; \mathbf{0}, \tilde{\boldsymbol{\Sigma}}_l) \prod_{l=d+1}^{n_1} \mathcal{PN}(\tilde{\mathbf{y}}_l; \mathbf{0}, \sigma_0^2 \mathbf{I}_{n_1}), \quad (4)$$

where $\tilde{\mathbf{y}}_l = (\mathbf{Y} - \mathbf{M})^T \mathbf{a}_l$ for $l = 1, \dots, d$, and $\tilde{\mathbf{y}}_l = (\mathbf{Y} - \mathbf{M})^T \mathbf{a}_l$ with \mathbf{a}_l being the $(l - d)$ th column of \mathbf{A}_c for $l = d+1, \dots, n_1$, $\tilde{\boldsymbol{\Sigma}}_l = \boldsymbol{\Sigma}_l + \sigma_0^2 \mathbf{I}_{n_2}$ and $\mathcal{PN}(\cdot; \boldsymbol{\mu}, \boldsymbol{\Sigma})$ denotes the density of the multivariate normal distribution with mean $\boldsymbol{\mu}$ and covariance matrix $\boldsymbol{\Sigma}$. In practice, note that we can avoid computing \mathbf{A}_c by using the identity $\mathbf{A}_s \mathbf{A}_s^T + \mathbf{A}_c \mathbf{A}_c^T = \mathbf{I}_{n_1}$. The derivation of Equation (4) is given in the supplementary materials.

The orthogonal factor loading matrix in Assumption 1 and prior independence of factor processes lead to the posterior independence of the factor processes, introduced in the following corollary.

Corollary 1. *For model (1) with Assumption 1:*

1. *The covariance of the posterior marginal distributions of any two factor processes is zero: $\text{Cov}[\mathbf{Z}_l^T, \mathbf{Z}_m^T \mid \mathbf{Y}, \boldsymbol{\Theta}] = \mathbf{0}_{n_2 \times n_2}$, where $l = 1, \dots, d$, $m = 1, \dots, d$ and $l \neq m$.*
2. *For $l = 1, \dots, d$, the posterior distribution $(\mathbf{Z}_l^T \mid \mathbf{Y}, \boldsymbol{\Theta})$ follows a multivariate normal distribution*

$$\mathbf{Z}_l^T \mid \mathbf{Y}, \boldsymbol{\Theta} \sim \mathcal{N}(\boldsymbol{\mu}_{Z_l}, \boldsymbol{\Sigma}_{Z_l}), \quad (5)$$

where $\boldsymbol{\mu}_{Z_l} = \boldsymbol{\Sigma}_l \tilde{\boldsymbol{\Sigma}}_l^{-1} \tilde{\mathbf{y}}_l$ and $\boldsymbol{\Sigma}_{Z_l} = \boldsymbol{\Sigma}_l - \boldsymbol{\Sigma}_l \tilde{\boldsymbol{\Sigma}}_l^{-1} \boldsymbol{\Sigma}_l$ with $\tilde{\boldsymbol{\Sigma}}_l = \boldsymbol{\Sigma}_l + \sigma_0^2 \mathbf{I}_{n_2}$.

We call the latent factor processes in (1) with Assumption 1 *Gaussian orthogonal latent factor* (GOLF) processes, because of orthogonal decomposition of the likelihood function and posterior independence between two factor processes. The main idea is to decompose the likelihood of GP models with multi-dimensional inputs by a product of densities with low dimension input and to utilize the continuous-time Kalman filter for fast computation. As we will see in Section 3, these two properties dramatically ease the computational burden.

2.2 Flexible mean function and marginalization

The mean function $m_s(\cdot)$ plays an important role in modeling and predicting correlated data. Computer models (such as the numerical solution of partial differential equations),

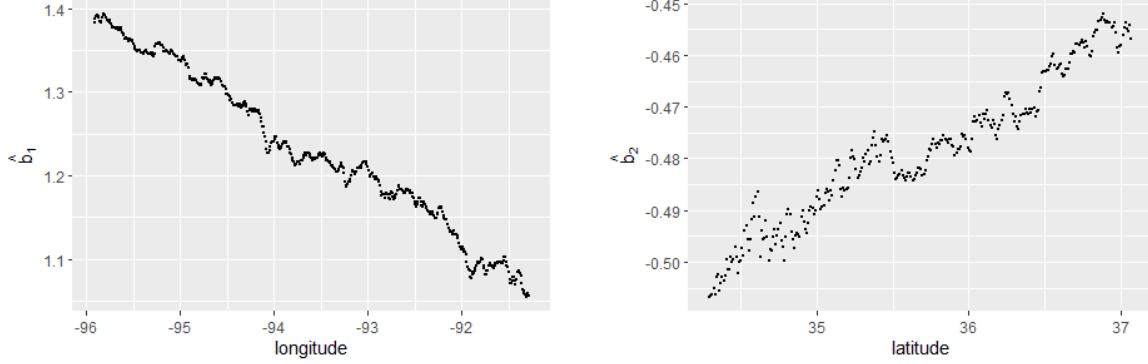


Figure 1: Estimated linear coefficients for temperature observations in Heaton et al. (2019). In the left panel, the dots are the estimated coefficients in a linear regression of observations at each longitude separately using latitudes as regressors. The estimated linear coefficients for the observations at each latitude are graphed in the right panel, where longitudes are used as regressors.

for example, can be included as a part of the mean in an inverse problem (Kennedy and O’Hagan, 2001). Here for simplicity, we use only a linear basis function of \mathbf{s} and \mathbf{x} , whereas additional terms may be included in the mean if available.

In a GP model, the regression coefficients are often assumed to be the same across one basis function. For instance, the mean function may be modeled as $\mathbf{m}_s(\mathbf{x}) = \mathbf{h}_1(\mathbf{s})\mathbf{b}_{1,0}$, or $\mathbf{m}_s(\mathbf{x}) = \mathbf{h}_2(\mathbf{x})\mathbf{b}_{2,0}$, where $\mathbf{h}_1(\mathbf{s})$ and $\mathbf{h}_2(\mathbf{x})$ are a set of $1 \times q_1$ and $1 \times q_2$ mean basis functions with $\mathbf{b}_{1,0}$ and $\mathbf{b}_{2,0}$ being $q_1 \times 1$ and $q_2 \times 1$ regression coefficients, respectively. The regression coefficients $\mathbf{b}_{1,0}$, for example, are shared across each \mathbf{x} .

The shared regression coefficients may be a restrictive assumption when data sets are large. Consider, for instance, the temperature data set used in Heaton et al. (2019), where the temperature values are shown in Figure 5. In Figure 1, we graph the fitted linear regression coefficients using latitudes or longitudes as regressors. The estimated regression coefficients are not the same across latitude or longitude. A natural extension of modeling the mean function, therefore, is to allow the mean parameters at each row or column of the observations to be different, e.g. $\mathbf{m}_{s_i}(\mathbf{x}_j) = \mathbf{h}_1(\mathbf{s}_i)\mathbf{b}_{1,j}$, or $\mathbf{m}_{s_i}(\mathbf{x}_j) = \mathbf{h}_2(\mathbf{x}_j)\mathbf{b}_{2,i}$, for $i = 1, \dots, n_1$ and $j = 1, \dots, n_2$. Some choices of the individual mean functions are summarized in Table 1. The mean function may be specified based on model interpretation or exploratory data analysis. Models with different regression coefficients across different types of coordinates are more suitable to model a large number of observations, as they are more flexible to capture the trend.

To implement full Bayesian inference of the parameters, one may sample from the posterior distribution of regression parameters $p(\mathbf{B} \mid \boldsymbol{\Theta}_{-B}, \mathbf{Y}, \mathbf{Z})$. However, we found a severe identifiability problem between the mean \mathbf{M} and \mathbf{AZ} , when the regression coefficients \mathbf{B} are sampled from the full posterior distribution. This is because the likelihood function of the mean parameters is flat when data are very correlated. Consequently, the absolute values of the entries of these two matrices can be both big, making the MCMC algorithm very unstable. To alleviate the identifiability problem, we first integrate out factors and sample regression parameters from the marginal posterior distribution $p(\mathbf{B} \mid \boldsymbol{\Theta}_{-B}, \mathbf{Y})$. The marginal

Individual mean	$\mathbf{m}_{s_i}(\mathbf{x}_j)$	\mathbf{M}	coefficients \mathbf{B}
Linear trend of \mathbf{s}	$\mathbf{h}_1(\mathbf{s}_i)\mathbf{b}_{1,j}$	$\mathbf{H}_1\mathbf{B}_1$	\mathbf{B}_1
Linear trend of \mathbf{x}	$\mathbf{h}_2(\mathbf{x}_j)\mathbf{b}_{2,i}$	$(\mathbf{H}_2\mathbf{B}_2)^T$	\mathbf{B}_2
Mixed linear trend	$\mathbf{h}_1(\mathbf{s}_i)\mathbf{b}_{1,j} + \mathbf{h}_2(\mathbf{x}_j)\mathbf{b}_{2,i}$	$\mathbf{H}_1\mathbf{B}_1 + (\mathbf{H}_2\mathbf{B}_2)^T$	$[\mathbf{B}_1, \mathbf{B}_2]$

Table 1: Summary of the mean function studied in this work. In the third column, $\mathbf{H}_1 = (\mathbf{h}_1^T(\mathbf{s}_1), \dots, \mathbf{h}_1^T(\mathbf{s}_{n_1}))^T$ and $\mathbf{H}_2 = (\mathbf{h}_2^T(\mathbf{x}_1), \dots, \mathbf{h}_2^T(\mathbf{x}_{n_2}))^T$ are $n_1 \times q_1$ and $n_2 \times q_2$ mean basis matrices, respectively. Regression coefficients are denoted as $\mathbf{B}_1 = (\mathbf{b}_{1,1}, \dots, \mathbf{b}_{1,n_2})$ and $\mathbf{B}_2 = (\mathbf{b}_{2,1}, \dots, \mathbf{b}_{2,n_1})$ for the basis function $\mathbf{h}_1(\cdot)$ and $\mathbf{h}_2(\cdot)$, respectively.

posterior distributions of the regression parameters are given in the following Theorem 1 and Theorem 2.

Theorem 1. 1. (Row regression coefficients). Assume $\mathbf{M} = \mathbf{H}_1\mathbf{B}_1$ and the objective prior $\pi(\mathbf{B}_1) \propto 1$ for \mathbf{B}_1 . After marginalizing out the factor \mathbf{Z} , the posterior samples of \mathbf{B}_1 from $p(\mathbf{B}_1 \mid \mathbf{Y}, \boldsymbol{\Theta}_{-\mathbf{B}_1})$ can be obtained by

$$\mathbf{B}_1 = \hat{\mathbf{B}}_1 + (\mathbf{H}_1^T \mathbf{H}_1)^{-1} \mathbf{H}_1^T \mathbf{A}_s \tilde{\mathbf{B}}_{1,0,s}^T + \sigma_0 (\mathbf{H}_1^T \mathbf{H}_1)^{-1} \mathbf{H}_1^T (\mathbf{I}_{n_1} - \mathbf{A}_s \mathbf{A}_s^T) \mathbf{Z}_{0,1} \quad (6)$$

where $\hat{\mathbf{B}}_1 = (\mathbf{H}_1^T \mathbf{H}_1)^{-1} \mathbf{H}_1^T \mathbf{Y}$, $\tilde{\mathbf{B}}_{1,0,s}$ is an $n_2 \times d$ matrix with the l th column independently sampled from $\mathcal{N}(\mathbf{0}, \tilde{\boldsymbol{\Sigma}}_l)$ for $l = 1, \dots, d$, and $\mathbf{Z}_{0,1}$ is an $n_1 \times n_2$ matrix with each entry independently sampled from the standard normal distribution.

2. (Column regression coefficients). Assume $\mathbf{M} = (\mathbf{H}_2\mathbf{B}_2)^T$ and the objective prior $\pi(\mathbf{B}_2) \propto 1$ for the regression parameters \mathbf{B}_2 . After marginalizing out the factor \mathbf{Z} , the posterior samples of \mathbf{B}_2 from $p(\mathbf{B}_2 \mid \mathbf{Y}, \boldsymbol{\Theta}_{-\mathbf{B}_2})$ can be obtained by

$$\mathbf{B}_2 = \hat{\mathbf{B}}_2 + \tilde{\mathbf{B}}_{2,0,s} \mathbf{A}_s^T + \sigma_0 \mathbf{L}_{H_2} \mathbf{Z}_{0,2} (\mathbf{I}_{n_1} - \mathbf{A}_s \mathbf{A}_s^T), \quad (7)$$

where $\hat{\mathbf{B}}_2 = \sum_{l=1}^d (\mathbf{H}_2^T \tilde{\boldsymbol{\Sigma}}_l^{-1} \mathbf{H}_2)^{-1} \mathbf{H}_2^T \tilde{\boldsymbol{\Sigma}}_l^{-1} \mathbf{Y}^T \mathbf{a}_l \mathbf{a}_l^T + (\mathbf{H}_2^T \mathbf{H}_2)^{-1} \mathbf{H}_2^T \mathbf{Y}^T (\mathbf{I}_{n_1} - \mathbf{A}_s \mathbf{A}_s^T)$ and $\tilde{\mathbf{B}}_{2,0,s}$ is a $q_2 \times d$ matrix with the l th column independently sampled from $\mathcal{N}(\mathbf{0}, (\mathbf{H}_2^T \tilde{\boldsymbol{\Sigma}}_l^{-1} \mathbf{H}_2)^{-1})$ for $l = 1, \dots, d$. \mathbf{L}_{H_2} is a $q_2 \times q_2$ matrix such that $\mathbf{L}_{H_2} \mathbf{L}_{H_2}^T = (\mathbf{H}_2^T \mathbf{H}_2)^{-1}$ and $\mathbf{Z}_{0,2}$ is a $q_2 \times n_1$ matrix with each entry independently sampled from the standard normal distribution.

When both the row regression coefficients and column regression coefficients are in the model, we found that $\mathbf{M}_1 = \mathbf{H}_1\mathbf{B}_1$ and $\mathbf{M}_2 = (\mathbf{H}_2\mathbf{B}_2)^T$ are not identifiable, if we sample \mathbf{B}_1 and \mathbf{B}_2 from the full conditional distribution. To avoid this problem, we first marginalizing out \mathbf{B}_2 and \mathbf{Z} to sample \mathbf{B}_1 and then we condition \mathbf{B}_1 to sample \mathbf{B}_2 .

Theorem 2. Assume $\mathbf{M} = \mathbf{H}_1\mathbf{B}_1 + (\mathbf{H}_2\mathbf{B}_2)^T$ and let the objective prior $\pi(\mathbf{B}_1, \mathbf{B}_2) \propto 1$ for the regression parameters \mathbf{B}_1 and \mathbf{B}_2 .

1. After marginalizing out \mathbf{Z} and \mathbf{B}_2 , the marginal posterior sample of \mathbf{B}_1 from $p(\mathbf{B}_1 \mid \mathbf{Y}, \boldsymbol{\Theta}_{-\mathbf{B}_1, -\mathbf{B}_2})$ can be obtained by

$$\mathbf{B}_1 = \hat{\mathbf{B}}_1 + (\mathbf{H}_1^T \mathbf{H}_1)^{-1} \mathbf{H}_1^T \mathbf{A}_s \tilde{\mathbf{B}}_{1,Q}^T + \sigma_0 (\mathbf{H}_1^T \mathbf{H}_1)^{-1} \mathbf{H}_1^T (\mathbf{I}_{n_1} - \mathbf{A}_s \mathbf{A}_s^T) \mathbf{Z}_{0,1} \mathbf{P}_0, \quad (8)$$

where $\hat{\mathbf{B}}_1 = (\mathbf{H}_1^T \mathbf{H}_1)^{-1} \mathbf{H}_1^T \mathbf{Y}$, $\tilde{\mathbf{B}}_{1,Q}$ is an $n_2 \times d$ matrix with the l th column independently sampled from $\mathcal{N}(\mathbf{0}, \mathbf{Q}_{1,l})$, with $\mathbf{Q}_{1,l} = \mathbf{P}_l \tilde{\Sigma}_l^{-1} \mathbf{P}_l$ where $\mathbf{P}_l = \mathbf{I}_{n_2} - \mathbf{H}_2 (\mathbf{H}_2^T \tilde{\Sigma}_l^{-1} \mathbf{H}_2)^{-1} \mathbf{H}_2^T \tilde{\Sigma}_l^{-1}$ for $l = 1, \dots, d$. $\mathbf{Z}_{0,1}$ is an $n_1 \times n_2$ matrix with each entry independently sampled from standard normal distribution and $\mathbf{P}_0 = (\mathbf{I}_{n_2} - \mathbf{H}_2 (\mathbf{H}_2^T \mathbf{H}_2)^{-1} \mathbf{H}_2^T)$.

2. Posterior samples of \mathbf{B}_2 from $p(\mathbf{B}_2 \mid \mathbf{Y}_{B_1}, \Theta_{-B_2})$ can be obtained through equation (7) by replacing \mathbf{Y} by $\mathbf{Y} - \mathbf{H}_1 \mathbf{B}_1$.

In Theorem 1 and Theorem 2, the marginal posterior distribution of the regression coefficients depends on the $n_1 \times d$ factor loading matrix, but not the complement of the factor loading matrix (\mathbf{A}_c). Since we do not need to compute \mathbf{A}_c , the most computationally intensive terms are those containing the covariance matrix Σ_l and its inverse. Fortunately, each term can be computed with linear complexity with respect to n_2 instead of n_2^3 when the Matérn covariance is used, discussed in Section 3.2.

2.3 Spatial latent factor loading matrix

This section discusses a model of the latent factor loading matrix \mathbf{A}_s that satisfies the orthogonal constraint in (3). As output values are marginally correlated at two inputs \mathbf{s}_a and \mathbf{s}_b , a natural choice is to let \mathbf{A}_s be the eigenvectors corresponding to the largest d eigenvalues in the eigendecomposition of the correlation matrix \mathbf{R}_s , where the (i, j) th entry is specified by a kernel function $K_s(\mathbf{s}_i, \mathbf{s}_j)$, for $1 \leq i, j \leq n_1$. We give a few examples of models that can be written as special cases of the GOLF model when the \mathbf{A}_s is specified as eigenvectors of \mathbf{R}_s . For simplicity, we assume the mean is zero. The first and second classes of models are the GP models with separable covariance functions of input with two dimensions and three dimensions, respectively.

Example 1 (Spatial model with separable covariance). *Consider a spatial model of \mathbf{Y} at a regular $n_1 \times n_2$ lattice, where the (i, j) th input is (s_i, x_j) with s_i and x_j denoting the i th latitude coordinate and j th longitude coordinate, respectively. Assume the covariance of the spatial process is separable, meaning that $\mathbf{Y} \sim \mathcal{N}(\mathbf{0}, \sigma^2 \mathbf{R}_s \otimes \mathbf{R}_x + \sigma_0^2 \mathbf{I}_{n_1 n_2})$, where the (l_1, m_1) term of \mathbf{R}_s is parameterized by the kernel function $K_s(s_{l_1}, s_{m_1})$ and the (l_2, m_2) term of \mathbf{R}_x is $K_x(x_{l_2}, x_{m_2})$ for $1 \leq l_1, m_1 \leq n_1$ and $1 \leq l_2, m_2 \leq n_2$. Let $\mathbf{R}_s = \mathbf{U}_s \mathbf{\Lambda}_s \mathbf{U}_s^T$, where \mathbf{U}_s is a matrix of eigenvectors and $\mathbf{\Lambda}_s$ is a diagonal matrix of eigenvalues of \mathbf{R}_s with the l th diagonal term λ_l . The density of this spatial model is equivalent to model (1) with $\mathbf{A}_s = \mathbf{U}_s$, $\Sigma_l = \sigma^2 \lambda_l \mathbf{R}_x$ and $d = n_1$.*

Example 2 (Spatio-temporal model with separable covariance). *Consider a spatio-temporal model of \mathbf{Y} at $n_{1,1} \times n_{1,2} \times n_2$ lattice, where the (i, j, k) th input is $(s_{1,i}, s_{2,j}, x_k)$, with $s_{1,i}$ and $s_{2,j}$ denoting the i th latitude coordinate and j th longitude coordinate, respectively, and x_k denoting the k th time point. Let $n_1 = n_{1,1} \times n_{1,2}$. Assume the covariance of the spatio-temporal process is separable, meaning that $\mathbf{Y} \sim \mathcal{N}(\mathbf{0}, \sigma^2 \mathbf{R}_{s_1} \otimes \mathbf{R}_{s_2} \otimes \mathbf{R}_x + \sigma_0^2 \mathbf{I}_{n_1 \times n_2})$ with the (l_i, m_i) th term of \mathbf{R}_{s_i} parameterized by the kernel function $K_s(s_{l_i}, s_{m_i})$ with $1 \leq l_i, m_i \leq n_{1,i}$ for $i = 1, 2$, and the (l_3, m_3) th term of \mathbf{R}_x being $K_x(x_{l_3}, s_{m_3})$ with $1 \leq l_3, m_3 \leq n_2$. Let $\mathbf{R}_{s_i} = \mathbf{U}_i \mathbf{\Lambda}_i \mathbf{U}_i^T$ where \mathbf{U}_i is a matrix of eigenvectors and $\mathbf{\Lambda}_i$ is a diagonal matrix of eigenvalues λ_{l_i} for $1 \leq l_i \leq n_{1,i}$ and $i = 1, 2$. The density of this spatio-temporal model is equivalent*

to model (1) with $\mathbf{A}_s = \mathbf{U}_1 \otimes \mathbf{U}_2$, $\Sigma_l = \sigma^2 \lambda_{l_1} \lambda_{l_2} \mathbf{R}_x$ with $1 \leq l_i, m_i \leq n_{1,i}$ for $i = 1, 2$, $l = l_1 + (l_2 - 1)n_{1,2}$ and $d = n_1$.

The separable covariance is widely used in emulating and calibrating computationally expensive computer models with scalar output (Sacks et al., 1989) and vector output (Conti and O’Hagan, 2010; Paulo et al., 2012), whereas the isotropic covariance, i.e., the covariance as a function of Euclidean distance of inputs, is used more often in modeling spatially correlated data (Gelfand et al., 2010). Some anisotropic kernels, such as the geometrically anisotropic kernel, were studied in Zimmerman (1993) for modeling spatially correlated observations. Note that the covariance of GOLF processes in (1) is not separable in general, as the variance and kernel parameters of each factor process $z_l(\cdot)$ can be different. Different kernel parameters make the model more flexible, as the factor processes corresponding to large eigenvalues are often found to be smoother than the ones corresponding to small eigenvalues. Separable covariance may be restrictive in this regard as factor processes are assumed to have the same kernel and parameters.

Computing the likelihood of GP with separable covariance on a complete $n \times n$ lattice data generally takes $O(N^{3/2})$ operations through eigen-decomposition of sub covariance matrices. This work generalizes this approach to nonseparable covariance for both complete and incomplete lattice observations. One can further reduce the computational complexity by selecting d eigenvectors corresponding to the d largest eigenvectors from the eigendecomposition of the correlation matrix \mathbf{R}_s . The proportion of summation of the d largest eigenvalues over the summation of total eigenvalues shall be chosen as large as possible to allow the model to explain the most variability of the signal (Higdon et al., 2008). We found that using more factors than the truth typically will not incur a large reduction of predictive accuracy, whereas using a much smaller number of factors than the truth will cause a large predictive error (Example 4 in simulated studies). Thus one should be cautious about using a very small number of factors.

2.4 Kernel functions

We first discuss the kernel function for the factor process $Z_l(\cdot)$, $l = 1, \dots, d$. We assume a product kernel between the inputs (Sacks et al., 1989), i.e. for any input $\mathbf{x}_a = (x_{a1}, \dots, x_{ap_2})$ and $\mathbf{x}_b = (x_{b1}, \dots, x_{bp_2})$, $K_l(\mathbf{x}_a, \mathbf{x}_b) = \prod_{i=1}^{p_2} K_{l,i}(|x_{ai} - x_{bi}|)$, where $K_{l,i}(\cdot)$ is a kernel of the l th coordinate of the input for $l = 1, \dots, d$ and $i = 1, \dots, p_2$.

We focus on Matérn covariance (Handcock and Stein, 1993) as kernel function $K_{l,i}(\cdot)$ in this work. Each kernel contains positive roughness parameter $\nu_{l,i}$ and a nonnegative range parameter $\gamma_{l,i}$ for $l = 1, \dots, d$ and $i = 1, \dots, p_2$. The roughness parameter of the Matérn kernel controls the smoothness of the process. When $\nu_{l,i} = \frac{1}{2}$, the Matérn kernel becomes the exponential kernel: $K_{l,i}(|x_{ai} - x_{bi}|) = \exp(-|x_{ai} - x_{bi}|/\gamma_{l,i})$, and when $\nu_{l,i} \rightarrow \infty$, the Matérn kernel becomes the Gaussian kernel: $K_{l,i}(|x_{ai} - x_{bi}|) = \exp(-|x_{ai} - x_{bi}|^2/(2\gamma_{l,i}^2))$. The half-integer Matérn kernel (i.e. $(2\nu_{l,i} + 1)/2 \in \mathbb{N}$) has a closed form expression. When $\nu_{l,i} = 5/2$, for example, the Matérn kernel is

$$K_{l,i}(|x_{ai} - x_{bi}|) = \left(1 + \frac{\sqrt{5}|x_{ai} - x_{bi}|}{\gamma_{l,i}} + \frac{5|x_{ai} - x_{bi}|^2}{3\gamma_{l,i}^2}\right) \exp\left(-\frac{\sqrt{5}|x_{ai} - x_{bi}|}{\gamma_{l,i}}\right), \quad (9)$$

for $l = 1, \dots, d$ and $i = 1, \dots, p_2$.

In constructing GOLF processes, we decompose the density of the GP model with multi-dimensional input into a product of the orthogonal components with lower-dimensional input. This is because the likelihood and the predictive distribution of a GP model with a half-integer Matérn covariance can be computed through linear operations with respect to the sample size by the continuous-time Kalman filter (Särkkä and Hartikainen, 2012) when $p_2 = 1$. The computational advantage will be discussed in Section 3.2.

For the factor loading matrix, we let \mathbf{A}_s be the first d eigenvectors of \mathbf{R}_s . The kernel functions for \mathbf{R}_s can be chosen similarly as the kernel for the latent factor processes. Without the loss of generality, we assume \mathbf{R}_s is parameterized by a product kernel with the range parameters γ_0 , and the Matérn kernel being used for each coordinate of \mathbf{s} .

3 Posterior sampling for GOLF processes

3.1 A Markov chain Monte Carlo approach

In many applications, the observations contain missing values. Denote \mathbf{Y}_v^o and \mathbf{Y}_v^u the vectors of observed data and missing data in matrix \mathbf{Y} with size N_o and N_u , respectively. Directly computing the likelihood includes calculating the inverse and determinant of an $N_o \times N_o$ covariance matrix, which has computational operations $O(N_o^3)$ in general, making it infeasible for large number of observations. Here we discuss a computationally feasible way for the GOLF model when observations are from incomplete matrices.

We start with a set of initial values at the locations with missing observations. Denote $\mathbf{Y}_v^{(t)} = \text{vec}(\mathbf{Y}^{(t)}) = [(\mathbf{Y}_v^o)^T, (\mathbf{Y}_v^{u,(t)})^T]^T$ an N -vector, where \mathbf{Y}_v^o and $\mathbf{Y}_v^{u,(t)}$ are vectors of observations and samples at the missing locations in the t th iteration, $t = 1, \dots, T$. First, we use a Metropolis algorithm to sample $\boldsymbol{\Theta}^{(t+1)}$ from the marginal posterior distribution $p(\boldsymbol{\Theta} \mid \mathbf{Y}^{(t)})$, where the marginal density is given in Equation (4). In the second step, we sample $\mathbf{Z}_l^{(t+1)}$ from $p(\mathbf{Z}_l^{(t+1)} \mid \mathbf{Y}^{(t)}, \boldsymbol{\Theta}^{(t+1)})$ by Equation (5) for $l = 1, \dots, d$, and then we generate $\mathbf{Y}^{(t+1)} = \mathbf{A}^{(t+1)}\mathbf{Z}^{(t+1)} + \mathbf{E}^{(t+1)}$, where $\mathbf{E}^{(t+1)}$ is an $n_1 \times n_2$ matrix of white noise with variance $\sigma_0^{(t+1)}$ and $\mathbf{A}^{(t+1)}$ is a $n_1 \times d$ matrix of the d eigenvectors corresponding to the d largest eigenvalues from the eigendecomposition of the correlation matrix \mathbf{R}_s in the $(t+1)$ th iteration. We can obtain $\mathbf{Y}_v^{u,(t+1)}$ by the last N_u terms in $\mathbf{Y}_v^{(t+1)}$, for $t = 1, \dots, T$. Note that the observed data \mathbf{Y}_v^o is never changed.

For computational reasons, we define the nugget parameter in each kernel (i.e. the inverse of the signal variance to the noise variance ratio parameter) $\eta_l = \sigma_0^2/\sigma_l^2$ for $l = 1, 2, \dots, d$, and the inverse range parameter $\beta_{l,i} = 1/\gamma_{l,i}$, where $i = 1, \dots, p_1$ when $l = 0$, and $i = 1, \dots, p_2$ when $l \geq 1$. The transformed parameters $\tilde{\boldsymbol{\Theta}}$ contain the mean parameters \mathbf{B} , inverse range parameters $\boldsymbol{\beta} = (\boldsymbol{\beta}_0, \dots, \boldsymbol{\beta}_d)$, nugget parameters $\boldsymbol{\eta} = (\eta_1, \dots, \eta_d)$ of the factor processes and the variance of the noise σ_0^2 .

For mean and noise variance parameters, we use an objective prior $\pi^R(\mathbf{B}, \sigma_0^2) \propto 1/\sigma_0^2$. We assume the jointly robust (JR) prior for the kernel parameters: $\pi^{JR}(\boldsymbol{\beta}_l, \eta_l) \propto (\sum_{i=1}^{p_2} (c_{l,2}\beta_{l,i} + \eta_l))^{c_{l,1}} \exp(-c_{l,3} \sum_{i=1}^{p_2} (c_{l,1}\beta_{l,i} + \eta_l))$ with default parameters $c_{l,1} = 1/2 - p_2$, $c_{l,2} = 1/2$, and $c_{l,3}$ being the average distance between the l th coordinate of two inputs for $l = 1, \dots, d$ (Gu, 2018). Note here $c_{l,1} = 1/2 - p_2$ is the default parameter for the MCMC algorithm, whereas

Algorithm 1 MCMC algorithm when the kernel parameters are different

- (1) For $l = 1, \dots, d$, sample $(\beta_l^{(t+1)}, \eta_l^{(t+1)})$ from $p(\beta_l, \eta_l \mid \tilde{\mathbf{y}}_l^{(t)})$.
 - (2) Sample $\beta_0^{(t)}$ from $p(\beta_0^{(t)} \mid \mathbf{Y}^{(t)}, \beta_{1:d}^{(t+1)}, \boldsymbol{\eta}_{1:d}^{(t+1)}, \mathbf{B}^{(t)})$.
 - (3) Sample $\sigma_0^{(t+1)}$ from $p(\sigma_0^{(t+1)} \mid \mathbf{Y}^{(t)}, \beta^{(t+1)}, \boldsymbol{\eta}^{(t+1)}, \mathbf{B}^{(t)})$.
 - (4) Sample $\mathbf{B}^{(t+1)}$ from $p(\mathbf{B}^{(t+1)} \mid \mathbf{Y}^{(t)}, \beta^{(t+1)}, \boldsymbol{\eta}^{(t+1)})$. Update the mean matrix $\mathbf{M}^{(t+1)}$ and the projected observations $\tilde{\mathbf{y}}_l^{(t)} = (\mathbf{Y} - \mathbf{M}^{(t+1)})^T \mathbf{a}_l$.
 - (5) For $l = 1, \dots, d$, sample $\mathbf{Z}_l^{(t+1)}$ from $p(\mathbf{Z}_l^{(t+1)} \mid \tilde{\mathbf{y}}_l^{(t)}, \beta^{(t+1)}, \boldsymbol{\eta}^{(t+1)})$ by Corollary 1 and sample $\mathbf{Y}^{(t+1)}$ by model (1). Update $\mathbf{Y}_v^{u,(t+1)}$ by the last N_u terms in $\mathbf{Y}_v^{(t+1)}$ and let $\tilde{\mathbf{y}}_l^{(t+1)} = (\mathbf{Y}^{(t+1)} - \mathbf{M}^{(t+1)})^T \mathbf{a}_l$.
 - (6) Update the posterior $p(\beta_l^{(t+1)}, \eta_l^{(t+1)} \mid \tilde{\mathbf{y}}_l^{(t+1)})$ and go back to (1) when $t < T$.
-

this prior parameter is different if one maximizes the marginal posterior distribution. The jointly robust prior is equivalent to the inverse gamma prior when the input dimension is one without a nugget parameter. The inverse gamma prior is assumed for each coordinate of β_0 with shape and rate parameter being $-1/2$ and 1 , respectively. The JR prior can alleviate the potential numerical problem when the estimated range and nugget parameters are close to the boundary of the parameter space, as the density of the JR prior is close to zero at these scenarios. As the sample size is large, the bias inserted from the prior is small.

The MCMC algorithm of the GOLF model is given in Algorithm 1. In step (1) to step (4) of Algorithm 1, we marginalize out the factor processes to compute the posterior distribution of the parameters. This is critically important as we found severe identifiability problems between the mean matrix \mathbf{M} and \mathbf{AZ} if the parameters are sampled from the full conditional distributions. Moreover, after marginalizing out the factor processes, the covariance matrix of the distribution $\mathcal{PN}(\tilde{\mathbf{y}}_l; \mathbf{0}, \tilde{\boldsymbol{\Sigma}}_l)$ in (4) contains a nugget term, which makes the computation stable.

The Algorithm 1 can be easily modified for different scenarios. When the factor processes have the same covariance matrix, we can combine step (1) and step (2) to sample the shared kernel and nugget parameter. Step (4) may be skipped if one has zero-mean or modified if one has the shared regression coefficients in the model.

Denote $\boldsymbol{\Sigma}_l = \mathbf{L}_l \mathbf{L}_l^T$ where \mathbf{L}_l is a lower triangular matrix in the Cholesky decomposition of $\boldsymbol{\Sigma}_l$. We need to efficiently compute the terms $|\tilde{\boldsymbol{\Sigma}}_l|$, $\mathbf{L}_l^{-1} \mathbf{v}_l$, $\mathbf{L}_l \mathbf{v}_l$ for any real-valued vector $\mathbf{v}_l := (v_{l,1}, \dots, v_{l,n_2})^T$ and sample $(\mathbf{Z}_l^{(t+1)})^T$ from $p((\mathbf{Z}_l^{(t+1)})^T \mid \tilde{\mathbf{y}}_l^{(t)}, \beta^{(t+1)}, \boldsymbol{\eta}^{(t+1)})$ for $l = 1, \dots, d$. Direct computation of the Cholesky decomposition of $\boldsymbol{\Sigma}_l$ requires $O(n_2^3)$ computational operations for each $l = 1, \dots, d$. Luckily, for Matérn covariance with a half-integer roughness parameter and one-dimensional input, computing any of these terms only takes $O(n_2)$ operations without approximation.

3.2 Continuous-time Kalman filter

We briefly review the continuous-time Kalman filter algorithm and the connection between the Gaussian Markov random field and GP with Matérn covariance. The spectral density of the Matérn covariance with the half-integer roughness parameter was shown to be the same as a continuous-time autoregressive process defined as a stochastic differential equation (SDE)

(Whittle, 1963). Suppose the observations are $\tilde{\mathbf{y}}_l = (\tilde{y}_{l,1}, \dots, \tilde{y}_{l,n_2})^T$. For $j = 1, \dots, n_2$ and $l = 1, \dots, d$, starting from the initial state $\boldsymbol{\theta}_l(s_0) \sim \text{MN}(\mathbf{0}, \mathbf{W}_l(s_0))$, the solution of the SDE follows (Hartikainen and Sarkka, 2010):

$$\begin{aligned}\tilde{y}_{l,j} &= \mathbf{F}\boldsymbol{\theta}_l(x_j) + \epsilon_{l,j}, \\ \boldsymbol{\theta}_l(x_j) &= \mathbf{G}_l(x_{j-1})\boldsymbol{\theta}_l(x_{j-1}) + \mathbf{w}_l(x_j),\end{aligned}\tag{10}$$

where $\mathbf{w}_l(x_j) \sim \mathcal{N}(\mathbf{0}, \mathbf{W}_l(s_j))$, $\epsilon_{l,j}$ is an independent white noise for $l = 1, \dots, d$ and $j = 1, \dots, n_2$. For the Matérn kernel with a half-integer roughness parameter, the terms $\mathbf{G}_l(x_j)$, $\mathbf{W}_l(x_j)$, and \mathbf{F} can be expressed explicitly as a function of $|x_j - x_{j-1}|$ and the range parameter of the kernel. Thus, the forward filtering and backward smoothing algorithm (FFBS) can be applied to compute the likelihood and to make predictions with linear computational operations of the number of observations (see e.g. Chapter 4 in West and Harrison (1997) and Chapter 2 in Petris et al. (2009) for the FFBS algorithm). The likelihood function and predictive distribution of a GP model having the Matérn kernel with roughness parameters being $1/2$ and $5/2$ through the FFBS algorithm are implemented in **FastGaSP** package available at CRAN. The computational complexity of the FFBS algorithm is only $O(n_2)$, with n_2 being the number of observations.

We briefly discuss how to apply the FFBS algorithm to compute terms $\mathbf{L}_l^{-1}\tilde{\mathbf{y}}_l$ and $|\tilde{\boldsymbol{\Sigma}}_l|$ needed in Algorithm 1, for $l = 1, \dots, d$. In the FFBS algorithm, the one-step-ahead predictive distribution $(\tilde{y}_{l,j} \mid \tilde{y}_{l,1:j-1}) \sim \mathcal{N}(f_l(x_j), Q_l(x_j))$ can be derived iteratively for $j = 1, \dots, n_2$ and for each $l = 1, \dots, d$. Closed form expressions of $f_l(x_j)$ and $Q_l(x_j)$ for the Matérn covariance in (9) are given in Gu and Xu (2020). For $l = 1, \dots, d$, we have following expressions for the computational expensive terms in the likelihood function:

$$|\tilde{\boldsymbol{\Sigma}}_l| = \prod_{j=1}^{n_2} Q_l(x_j), \quad \text{and} \quad \mathbf{L}_l^{-1}\tilde{\mathbf{y}}_l = \left(\frac{\tilde{y}_{l,1} - f_{l,1}}{\sqrt{Q_l(x_1)}}, \dots, \frac{\tilde{y}_{l,n_2} - f_{l,n_2}}{\sqrt{Q_l(x_{n_2})}} \right)^T.$$

We use the backward sampling algorithm (Petris et al., 2009) to sample $\boldsymbol{\theta}_{l,n_2}$ from $p(\boldsymbol{\theta}_{l,n_2} \mid \tilde{\mathbf{y}}_l^{(t)}, \boldsymbol{\beta}^{(t+1)}, \boldsymbol{\eta}^{(t+1)})$ and $\boldsymbol{\theta}_{l,j}$ from $p(\boldsymbol{\theta}_{l,j} \mid \tilde{\mathbf{y}}_l^{(t)}, \boldsymbol{\theta}_{l,j+1}, \boldsymbol{\beta}^{(t+1)}, \boldsymbol{\eta}^{(t+1)})$ sequentially, for $j = n_2 - 1, \dots, 1$. Posterior samples $\mathbf{Z}_l^T = (\mathbf{z}_l(x_1), \dots, \mathbf{z}_l(x_{n_2}))^T$ can be obtained by the first entry of the posterior sample $\boldsymbol{\theta}_{l,j}$ from the backward sampling algorithm, for $j = 1, \dots, n_2$. Furthermore, for any $n_2 \times 1$ real vector \mathbf{v}_l , we have $\mathbf{L}_l\mathbf{v}_l = (f_{l,1} + \sqrt{Q_l(x_1)}v_{l,1}, \dots, f_{l,n_2} + \sqrt{Q_l(x_{n_2})}v_{l,n_2})^T$ for $l = 1, \dots, d$ and $j = 1, \dots, n_2$.

3.3 Computational complexity

Denote $p = p_1 \times p_2$ the total dimension of the inputs (\mathbf{s}, \mathbf{x}) and suppose the observational matrix is $n_1 \times n_2$ with irregular missing values, where $n_1 \leq n_2$ and $N = n_1 n_2$. We discuss the computational complexity for three scenarios with $p = 2$ (e.g. spatially correlated data), $p = 3$ (e.g. spatio-temporal data) and $p > 3$ (e.g. functional data).

When $p = 2$, the computational complexity of the GOLF model with the half-integer Matérn kernel is $O(Nd)$. First, we compute the first d eigenvectors of $\boldsymbol{\Sigma}_s$ to obtain \mathbf{A}_s , which has $O(n_1^2 d)$ operations (see e.g. Chapter 4.5.5 in Bai et al. (2000)). Second, computing the marginal likelihood and sampling the factor processes by the FFBS algorithm only cost

$O(n_2d)$ operations. The largest computational order is from the matrix multiplication $\tilde{\mathbf{Y}}^T = (\mathbf{Y} - \mathbf{M})^T \mathbf{A}_s$, which is at the order of $O(Nd)$.

For $p = 3$, we let $\mathbf{A}_s = \mathbf{A}_{s_1} \otimes \mathbf{A}_{s_2}$, where \mathbf{A}_{s_1} and \mathbf{A}_{s_2} are the first d_1 and d_2 eigenvectors of $n_{1,1} \times n_{1,1}$ matrix Σ_{s_1} and $n_{1,2} \times n_{1,2}$ matrix Σ_{s_2} , respectively, with $n_{1,1} \times n_{1,2} = n_1$ and $\Sigma_{s_1} \otimes \Sigma_{s_2} = \Sigma_s$. Without the loss of generality, assume $d_1 \leq d_2$ and $n_1 \leq n_2$. Let the total number of factor processes be $d = d_1 d_2$. The computational order of the GOLF model with a half-integer Matérn covariance function is $O(n_1 n_2 d_{max})$ where d_{max} is the maximum of d_1 and d_2 (noting this is smaller than $O(n_1 n_2 d)$). To see this, computing the eigendecomposition of Σ_{s_1} and Σ_{s_2} requires $O(d_1 n_{1,1}^2)$ and $O(d_2 n_{1,2}^2)$ operations, respectively. Second, using the FFBS algorithm to compute the marginal likelihood and to sample factor processes costs $O(d n_2)$ operations. At last, we do NOT directly compute $\mathbf{Y}^T \mathbf{A}_s$ as its computation operations are $O(Nd)$. Instead, we first write the observations as an $n_2 \times n_{1,2} \times n_{1,1}$ array \mathbf{Y}_{ar}^T , where the (i, j, k) th entry being the outcome at $(s_{1,i}, s_{2,j}, x_k)$. Then we do a 3-mode matrix product followed by a 2-mode matrix product $\tilde{\mathbf{Y}}_{ar}^T \times_3 \mathbf{A}_{s_1} \times_2 \mathbf{A}_{s_2}$ (Kolda and Bader, 2009), which has the computation operations $O(n_2 n_1 d_1)$ and $O(n_2 n_{1,2} d)$, respectively. Finally we concatenate the second and third dimensions of $\tilde{\mathbf{Y}}_{ar}^T$ to obtain the $n_2 \times d$ matrix $\tilde{\mathbf{Y}}^T$.

For the case when $p > 3$, there might be two scenarios. In the first scenario, the data are observed in an $n_{1,1} \times n_{1,2} \times \dots \times n_{1,k} \times n_2$ tensor with irregular missing values, where $n_{1,1} \times n_{1,2} \times \dots \times n_{1,k} = n_1$. In this scenario, the computation will be Nd_{max} , where d_{max} is the maximum of d_1, \dots, d_k with similar deduction for the case with $p = 3$. In the second scenario, we have $p_2 > 1$. Examples include emulating a computationally expensive computer output with multivariate output (Conti and O'Hagan, 2010; Paulo, 2005). In this case, the Kalman filter algorithm may not be applied, so the additional computational order is $O(n_2^3)$, when the covariance of the factor process is the same. If the covariance is not the same, we need to additionally compute the inverse of covariance matrices of d multivariate normal distributions, which is at the order of $O(d n_2^3)$.

In sum, the computational complexity of GOLF for all scenarios considered herein is much smaller than $O(N_o^3)$ from directly inverting the covariance matrices. Besides, a few steps in the MCMC algorithm can be computed in parallel, such as FFBS algorithm to compute the product of d marginal densities of projected output and the matrix multiplication $\tilde{\mathbf{Y}}^T = (\mathbf{Y} - \mathbf{M})^T \mathbf{A}_s$, to further reduce the computational complexity.

4 Comparison and connection with other related models

GOLF processes are closely connected to a wide range of approaches on approximating GPs for modeling large correlated data. Model (1) is a linear model of coregionalization (LMC) (Gelfand et al., 2004), where the factor loading matrix is parameterized by input variables. Another widely used model for multivariate functional data is the semiparametric latent factor model (SLFM) (Teh et al., 2005), where the factor loading matrix can be estimated by the principal component analysis (PCA) (Higdon et al., 2008). However, the linear subspace estimated by PCA is equivalent to maximum marginal likelihood estimator (MMLE) with independent factors (Tipping and Bishop (1999)), whereas the latent factors at different

input variables are assumed to be correlated. The MMLE of factor loadings with correlated factors was derived in (Gu and Shen, 2020), called the generalized probabilistic principal component analysis (GPPCA). Our approach has two distinctions. First, our approach applies to observations with irregular missing values, whereas the observations are required to be matrices in GPPCA. Second, both inputs \mathbf{s} and \mathbf{x} are used for estimation, whereas only the input in latent processes is used in GPPCA and predictions can be more accurate.

To overcome the computational bottleneck of GPs, we project observations on orthogonal coordinates in a GOLF model, as the complexity of computing the likelihood of GPs with Matérn covariances with one dimension input is fast by the continuous-time Kalman Filter. The computational complexity can be further reduced by only using factor processes with large eigenvalues. The reduced rank approach is used widely in modeling correlated data. For instance, the predictive process by a set of pre-specified knots was studied in Banerjee et al. (2008), and the multiresolution local bisquare functions were used in Cressie and Johannesson (2008). Limitations of the reduced-rank method are studied in Stein (2014). Note that even for the full rank covariance, the computational order of GOLF is much less than $O(N_o^3)$. The primary goal is not to propose a reduced rank model herein, but to reduce the computational complexity of a GP model with a full-rank, flexible covariance function through orthogonal projections.

Many other approximation methods for GPs follow the framework of Vecchia’s approximation (Katzfuss and Guinness, 2017; Vecchia, 1988). Vecchia’s approximation is a broad framework that assumes the sparsity of the inverse of Cholesky decomposition of the covariance matrix of the latent processes, where the key is on selecting the order of the latent variables and imposing sensible conditional independence assumptions between variables. GOLF processes with Matérn kernel is closely related to Vecchia’s approximation, in the sense that the model can be written as a vector autoregressive model with orthogonal factor loading matrix. Our way of computing likelihood and predictions based on the FFBS algorithm is exact, rather than an approximation to the likelihood function. We compare our approach with a few other methods that fall into the framework of Vecchia’s approximation in Section 6.1.

5 Simulated studies

We discuss two simulated examples in this section. We first study a simulated example with a small sample size to study the predictive performance and parameter inference between GOLF processes and the exact GP model by directly computing the inversion and determinant of the covariance matrix in the likelihood function. In the second simulated example, we generate observations from separable and nonseparable models to study the predictive performance of GOLF processes with a different number of factors, and with the same or different kernel parameters. For both examples, we implement $J = 100$ experiments in each scenario, and we generate $T = 5,000$ MCMC samples for each method with the first 20% of the samples used as the burn-in samples.

Denote $y_{i,j}^*$ the i th held-out data in the j th simulated experiment in each scenario, for $i = 1, \dots, n^*$ and $j = 1, \dots, J$. Let \hat{y}_{ij}^* and $CI_{ij}(95\%)$ be the predictive mean and 95% predictive credible interval of the i th held-out data at the j th experiment, respectively. For

both simulated examples, we record the root mean square error, the percentage of held-out observations percentage covered in the 95% predictive interval, and the average length of the 95% predictive interval of the j th experiment ($L_{CI_j}(95\%)$):

$$\text{RMSE}_j = \sqrt{\frac{\sum_{i=1}^{N^*} (\hat{y}_{ij}^* - y_{ij}^*)^2}{N^*}}, \quad (11)$$

$$P_{CI_j}(95\%) = \frac{1}{N^*} \sum_{i=1}^{N^*} 1\{y_{ij}^* \in CI_{ij}(95\%)\}, \quad (12)$$

$$L_{CI_j}(95\%) = \frac{1}{N^*} \sum_{i=1}^{N^*} \text{length}\{CI_{ij}(95\%)\}, \quad (13)$$

for $j = 1, \dots, J$. We compute average values of these three quantities over $J = 100$ simulations to evaluate each approach. A precise method should have a small average RMSE, $P_{CI}(95\%)$ close to the 95% nominal level, and short predictive interval lengths. Here we only consider the pairwise interval of responses at each coordinate as outputs are univariate on spatial or spatio-temporal domain. Simultaneous credible interval can be used for applications with multivariate responses (Sørbye and Rue, 2011).

Example 3 (GOLF processes and exact GP model). *Data are sampled from a zero-mean separable GP model with two-dimensional inputs at a 25×25 regular lattice in $[0, 1]^2$. Two missing patterns are considered, where the data are missing at random in the first case, and a disk in the centroid of the lattice is missing in the second case.*

We assume a small sample size in Example 3 because of the computational burden by the exact Gaussian process model. We use the unit-variance covariance matrix parameterized by the exponential kernel and the Matérn kernel in (9) to generate the data. The range parameters of Matérn kernel are chosen as $\gamma_0 = 1$ and $\gamma_1 = \dots = \gamma_d = 1/3$. The range parameters of exponential kernel are chosen to be $\gamma_0 = 4$ and $\gamma_1 = \dots = \gamma_d = 1$. All the range parameters, the variance of the kernel, and noise are estimated by each method based on the MCMC algorithm.

We compare GOLF processes and the exact GP model where the inverse and determinant of the covariance matrix are directly computed. Both models use the same prior and proposal distribution in the MCMC algorithm to sample the kernel parameters. Table 2 gives the predictive performance of both methods for three scenarios, where 50% and 20% of the output are missing at random in the first two scenarios, and approximately 20% of the output is missing in a disk in the centroid of the lattice in the third scenario. Graphs of the observed data, full data, predictions, and trace plots of the posterior samples in one simulation are given in the supplementary materials.

As shown in Table 2, both methods have accurate predictions and uncertainty assessment for all scenarios. Out-of-sample RMSE for predicting the held out observations is close to 0.1, the standard deviation of the noise. The 95% predictive confidence intervals cover around 95% of the held-out observations, and the average length of the predictive confidence interval is small. Predictions of both methods are more precise for the cases when the data are missing at random than the ones when a disk of output is missing in the centroid of the lattice, as the

Kernel	Missing value		GOLF			Exact GP model			Difference		
	Percentage	Pattern	RMSE	$P_{CI}(95\%)$	$L_{CI}(95\%)$	RMSE	$P_{CI}(95\%)$	$L_{CI}(95\%)$	$\Delta RMSE$	ΔL	ΔU
Matérn	50%	random	0.106	0.954	0.425	0.106	0.952	0.423	0.002	0.006	0.006
	20%	random	0.103	0.952	0.410	0.103	0.952	0.411	0.001	0.007	0.007
	20%	disk	0.108	0.909	0.430	0.108	0.913	0.431	0.005	0.008	0.009
Exp	50%	random	0.129	0.955	0.518	0.128	0.953	0.513	0.005	0.009	0.008
	20%	random	0.120	0.947	0.472	0.120	0.948	0.471	0.003	0.009	0.009
	20%	disk	0.156	0.941	0.602	0.154	0.946	0.605	0.013	0.019	0.019

Table 2: Comparison between the exact GP model and GOLF processes. $J = 100$ simulated experiments are conducted for each scenario. $\Delta RMSE = \frac{1}{J} \sum_{j=1}^J \Delta RMSE_j$ measures the average L_2 distance by the two methods, where $\Delta RMSE_j = (\frac{1}{N^*} \sum_{i=1}^{N^*} (\hat{y}_{ij,GOLF}^* - \hat{y}_{ij,GP}^*)^2)^{1/2}$ with $\hat{y}_{ij,GOLF}^*$ and $\hat{y}_{ij,GP}^*$ denote the predictive mean by GOLF processes and exact GP model, respectively. ΔL and ΔU measure the average absolute difference between the lower bound and upper bound of 95% predictive intervals of the GOLF processes and the exact GP model, respectively.

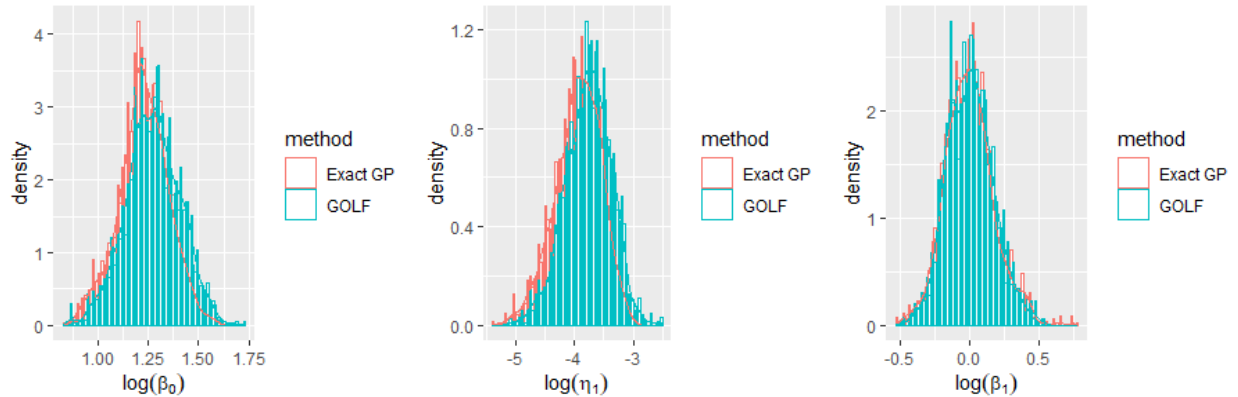


Figure 2: The histogram of posterior samples of the logarithm of the inverse range parameters and nugget parameters in one simulation of Example 3, where the data are generated using the Matérn kernel in (9) with 50% of the values missing at random.

estimated correlation between the held-out test output and nearby observations are relatively accurate.

For Example 3, note that GOLF processes and the exact GP model are the same with two different computational strategies. For GOLF processes, we sample the missing values to use the fast computational strategy, whereas the inverse and determinant of the covariance matrix are computed in the exact GP model directly. Therefore, the two different strategies have significantly different computational operations. The computational operations of GOLF processes is $O(Nd)$ with $N = n_1 \times n_2$ ($d = n_1$ in Example 3), whereas the computational operations of the exact GP model is $O(N_o^3)$, where N_o is the number of observations. Thus, GOLF processes are computationally feasible for a large data set. On the other hand, the difference in predictions and uncertainty assessment between the exact GP model and GOLF is small (last three columns in Table 2), since we do not make any approximation in computing GOLF processes.

Figure 2 shows the histogram of the 4000 after burn-in posterior samples from the GOLF processes and exact GP model in one simulation of Example 3. The posterior samples of the

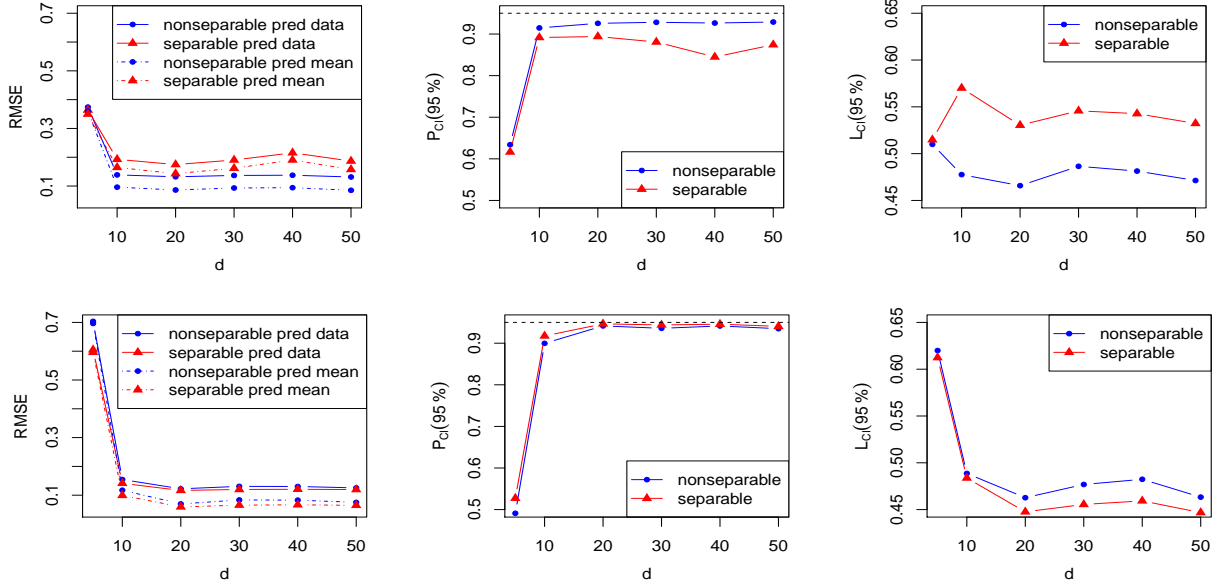


Figure 3: The predictive performance of GOLF process with $d = 5, 10, 20, 30, 40$ and 50 factors for Example 4. in the first row of panels, kernel parameters are different in simulating the data, whereas the parameters are the same in for simulation in the second row of panels. Blue curves and red curves denote the GOLF processes with different kernel parameters and the same kernel parameter, respectively. In the left panels, the solid curves denote the RMSE for predicting the (noisy) observations, and the dashed curve denotes the RMSE for predicting the mean of the observations. Proportions of observations covered in the 95% predictive interval and the average length of the predictive interval are graphed in the middle and right panels, respectively.

two methods are close to each other. The difference becomes even smaller when we increase the number of MCMC samples.

Example 4 (GOLF processes with different number of factors and kernel parameters). *The data are sampled from two scenarios with two-dimensional inputs being a 100×100 lattice in $[0, 1]^2$. In the first scenario, the range parameters of the kernel of each factor process are the same, whereas these parameters are chosen to be different in the second scenario. In both scenarios, a disk of output in the centroid of the lattice is masked out for testing, corresponding to approximately 20% of the total number of data. We use $d = 30$ (low-rank) and $d = 100$ (full-rank) factors to generate the data. We test GOLF processes with a different number of factors, same or different range parameters.*

In Example 4, the factor processes are assumed to have the Matérn kernel in (9) and unit variance. The kernel parameter is shared in the first scenario, where $\gamma_0 = 1/4$ and $\gamma_l = 1/2$, and in the second scenario $\gamma_0 = 1/3$ and $\gamma_l = 1/l$, for $l = 1, \dots, d$. We estimate these parameters through the posterior samples from the MCMC algorithm.

Predictive performance of different approaches for data simulated by $d = 30$ latent processes are graphed in Figure 3. In the first row of the panels, since data are simulated

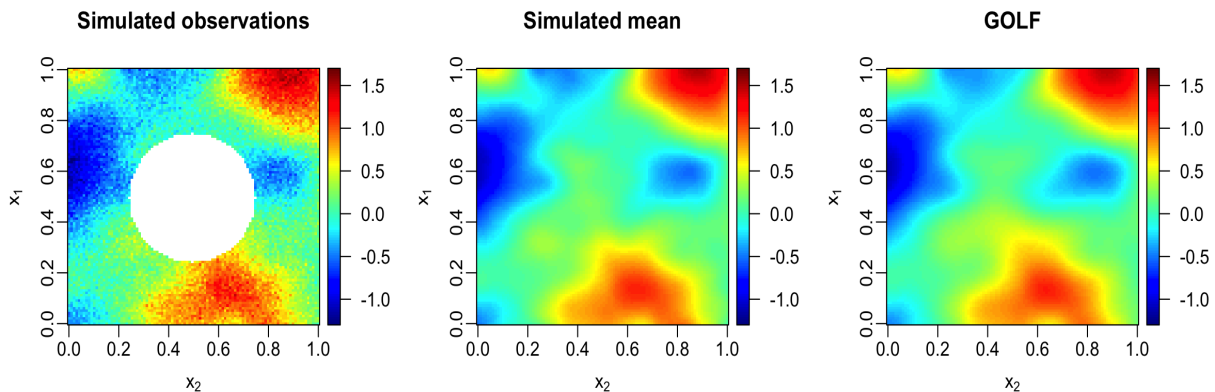


Figure 4: The left figure shows the observed data in one simulation of Example 4, where a disk of observations is missing. The middle figure contains the mean of the data and the right figure is the prediction from GOLF process.

by GOLF processes with different kernel parameters, nonseparable GOLF processes have smaller predictive RMSE and a shorter interval that covers almost 95% of the data. In the second row of the panels, GOLF processes with the same kernel parameter seem to be slightly better, as the true factor process has the same kernel parameter. The difference between the two methods in the second row is smaller, as the GOLF model with a separable kernel is a special case of the one with different kernel parameters.

From Figure 3, we found that when we use $d = 20$ factor processes or more, the predictive results seem to be similar, as the data are simulated using $d = 30$ factor processes. The way of selecting the number of factors is currently ad-hoc. One may select the number of factors to ensure a large proportion of the variance explained by the sum of the eigenvalues of the correlation matrix \mathbf{R}_s . This simulation suggests that using more factors may be better in prediction than using very few factors.

In Figure 4, we graph the simulated observations, simulated mean, and the prediction from the GOLF model with $d = 30$ in one simulation. Predictions look reasonably accurate. Results when the data are generated by a full rank kernel ($d = 100$) are provided in Figure S3 in supplementary materials. Results are very similar to Figure 3.

6 Real applications

6.1 Predicting large spatial data on an incomplete lattice

We compare GOLF processes with different approaches on predicting the missing temperature values in Heaton et al. (2019). This data set contains daytime land surface temperatures on August 4, 2016, at 300×500 spatial grids with the latitude and longitude ranging from 34.30 to 37.07, and from -95.91 to -91.28, respectively. The complete data set consists of 148,309 observations with 1,791 missing values due to cloud cover. The training data (plotted in the left panel in Figure 1) consists of 105,569 observations, whereas 42,740 observations were held out as the test data. Training observations and full observations are graphed in

Methods	RMSE	$P_{CI}(95\%)$	$L_{CI}(95\%)$	Run time (mins)
FRK	3.16	0.77	6.09	3.53
Gapfill	1.86	0.35	1.44	6.98
GOLF	1.46	0.92	4.95	48.6
LAGP	2.07	0.84	5.70	3.76
LatticeKrig	1.68	0.963	6.58	214.25
MRA	1.85	0.92	5.54	4.99
NNGP	1.64	0.95	5.84	1.14
Partition	1.80	0.82	4.56	827.37
SPDE	1.55	0.97	7.87	34.8

Table 3: Comparison for the dataset in Heaton et al. (2019). The standard deviation of observations is 4.07. For each method, we compute RMSE, $P_{CI}(95\%)$ and $L_{CI}(95\%)$ defined in (11)-(13). A satisfying method should have small RMSE and small $L_{CI}(95\%)$ and $P_{CI}(95\%)$ closed to be 95% nominal level. We compare the fixed rank kriging (FRK) (Cressie and Johannesson (2008)), the Gapfill method (Gerber et al. (2018)), GOLF processes, the local approximate Gaussian processes (LAGP) (Gramacy and Apley (2015)), the lattice kriging (LatticeKrig) (Nychka et al. (2015)), the multiresolution approximation (MRA) (Katzfuss (2017)), the nearest neighbor Gaussian processes (NNGP) (Datta et al. (2016)), the spatial partitioning (Partition) (Heaton et al. (2017)), and stochastic partial differential equations (SPDE) (Lindgren et al. (2011)).

the upper panel in Figure 5.

We define GOLF processes on this dataset with s being latitude and x being longitude. Since areas with higher latitude typically have lower temperature on average, we assume a mean parameter for each latitude value, i.e. $\mathbf{M} = (\mathbf{H}_2 \mathbf{B}_2)^T$, where $\mathbf{H}_2 = \mathbf{1}_{n_2}$ and $\mathbf{B}_2 = (b_{2,1}, \dots, b_{2,n_1})^T$. We let $d = n_1/2$ and use exponential kernels with distinct variances and range parameters sampled from the marginal posterior distribution for GOLF processes. We compute $M = 6000$ posterior samples where the first 20% were used as the burn-in samples. Results of longer MCMC chains and different initial values of the parameters are given in the supplementary materials.

In Heaton et al. (2019), 12 groups of researchers across the globe implemented their methods to predict missing temperature values for competition. Among this cohort of researchers are authors that conjured up some of the most popular methods for large spatially correlated data. Other than GOLF processes, we implement 8 of 12 approaches based on the code provided in (Heaton et al., 2019). We could not implement the other 4 approaches due to memory limitation of the computing facility or unavailability of the code. All computations are operated on a 3.60GHz 8 cores Intel i9 processor with 32 GB of RAM on a macOS Mojave operating system.

The predictive performance of different approaches is recorded in Table 3. Most of the results are consistent with what is shown in Heaton et al. (2019), whereas small differences remain for those requiring random starts or stochastic algorithms. E.g., 5 implementation of the SPDE method gives different RMSE ranging from 1.55 to 1.88. Besides, running time of some methods are slightly different. For SPDE and LatticeKrig, for instance, it takes 35

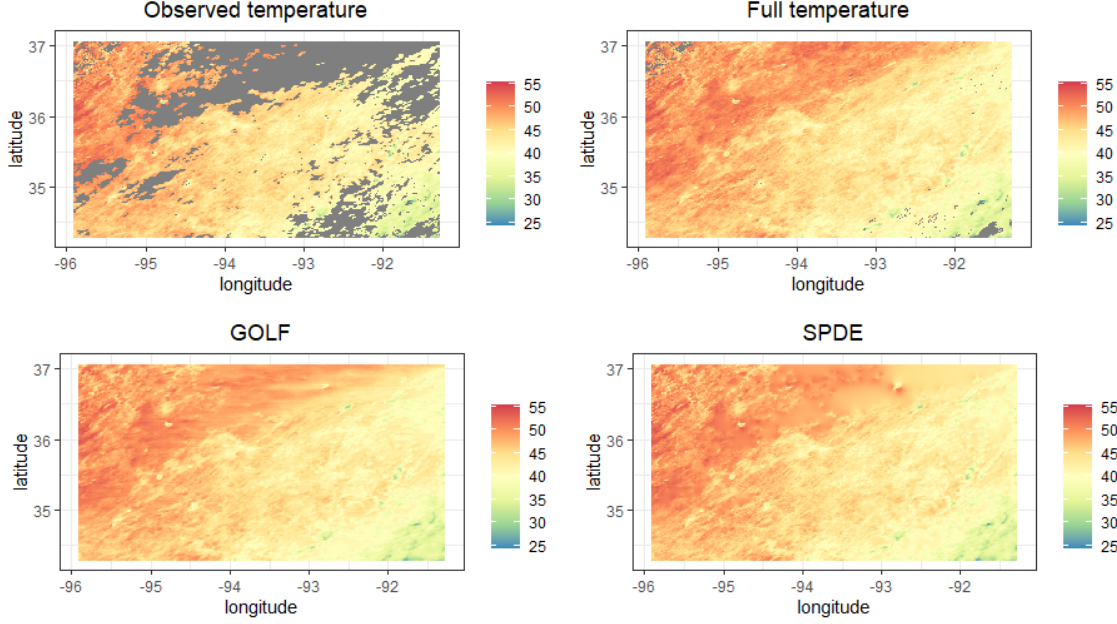


Figure 5: The top panels show the observed temperature and full temperature, respectively, where the gray area contains unobservable points. The bottom panel are the predictions from two methods, GOLF and SPDE, respectively.

mins and 214 mins to run in our system, respectively, whereas it takes 138 mins and 78 mins to run in Heaton et al. (2019), respectively.

We acknowledge that held-out observations were not released in Heaton et al. (2019), adding difficulty for model specification. The good performance of the GOLF model may be explained by two reasons. First, different mean parameters are assumed at each latitude, which is more flexible to capture information from a large number of observations. Second, we assume different range and variance parameters of the factor processes, which are more flexible than the separable or isotropic kernel functions.

The 95% predictive interval of the GOLF model is the shortest, and it covers around 92% of the held out test data, as shown in Table 3. In supplementary materials, we provide diagnostic plots of the fitted values from the GOLF model and predictive performance based on several configurations, including 40,000 MCMC samples and different initial parameters. The predictive performance of the GOLF model at different configurations is similar. Besides, the computational time of GOLF per one MCMC iteration is around 0.49s for this example, which is comparable to NNGP (0.53s) and faster than MRA (3.29s) for one iteration. The posterior sampling obtained here provided uncertainty quantification of model parameters, whereas most of the methods provided in Table 3 only provide a point estimator of the parameters. Future works are needed to reduce the number of iterations in GOLF to achieve a similar level of predictive accuracy.

The predictive mean of the GOLF processes and SPDE are graphed in the middle panel and right panel in Figure 5, respectively. Predictions from the GOLF processes are more accurate for predicting temperatures in areas with high latitude, possibly due to flexible mean parameters estimated from data. Both methods seem to be slightly oversmoothing.

Methods	RMSE	$P_{CI}(95\%)$	$L_{CI}(95\%)$	Run time (mins)
FRK	0.846	0.967	3.92	29.4
GOLF	0.325	0.942	1.08	43.9
LAGP	0.695	0.951	1.80	6.18
Spatial model 1	0.365	0.928	2.09	26.5
Spatial model 2	0.348	0.928	2.02	42.7

Table 4: Predictive performance of different approaches for the NOAA monthly gridded temperature dataset. The standard deviation of the outcomes in this dataset is 0.940. Results of the FRK, GOLF, and LAGP are given in the first to the third rows. For the results in the fourth and fifth rows, spatial models were fitted using the **RobustGaSP** package with one initial value and two initial values of the range and nugget parameters for finding their marginal posterior mode, respectively.

Yet predicting the missing values of this data set is challenging, as the observations are missing in spatial blocks. Both methods seem precise in prediction.

6.2 Analysis of large spatio-temporal data set

We consider the monthly gridded temperature anomalies from U.S. National Oceanic and Atmospheric Administration (NOAA) ¹. The data set contains the average air and marine temperate anomalies at 5 degrees longitude-latitude grids with respect to 1981-2010 base period. R code and examples to load NOAA gridded data can be found in Shen (2017). We compare the predictive performance using the data from Jan 1999 to Dec 2018. For each month, we observe the temperature anomalies at $n_1 = 36 \times 28$ spatial grids with longitude ranging from 182.5 to 357.5 and with latitude ranging from -62.5 to 72.5, respectively. There are 11,122 missing data, leaving the total number of observations to be 230,798. We held out 50% randomly sampled temperature anomalies as the missing data, and the rest 50% is used as training data (i.e., $n = n^* = 115,399$). Predicting the missing values in this scenario is more difficult than the example in (Gu and Shen, 2020), where the data are missing in a set of locations over the same months.

We fit the GOLF processes with the covariance of each spatial coordinate modeled by the Matérn covariance, and the factors processes are defined on the temporal input with different kernel parameters. Due to computational limitation, we let the number of factors be $d = 0.75^2 n_1 = 567$ and assume the factor loadings to be a Kronecker product of the first three-quarters of the eigenvectors of the sub-covariance matrices for longitude and latitude. Although we have a large number of factors, the computational complexity is $O(Nd_{max})$ with $d_{max} = 0.75 \times 36 = 48$ rather than $O(Nd_1d_2)$ by the mode multiplication of tensor (see Section 3.3 for the discussion). We assume the coefficients of the intercept and linear coefficients are different at each location, i.e. $\mathbf{M} = (\mathbf{H}_2\mathbf{B}_2)^T$ where $\mathbf{H}_2 = [\mathbf{1}_{n_2}, \mathbf{x}]$, with \mathbf{x} being 240 months and \mathbf{B}_2 being a matrix of $2 \times n_1$ coefficients. We use $M = 3000$ MCMC samples with the first 20% as the burn-in samples, as posterior samples converge at a small number of iterations in this example.

¹<ftp://ftp.ncdc.noaa.gov/pub/data/noaaglobaltemp/operational>

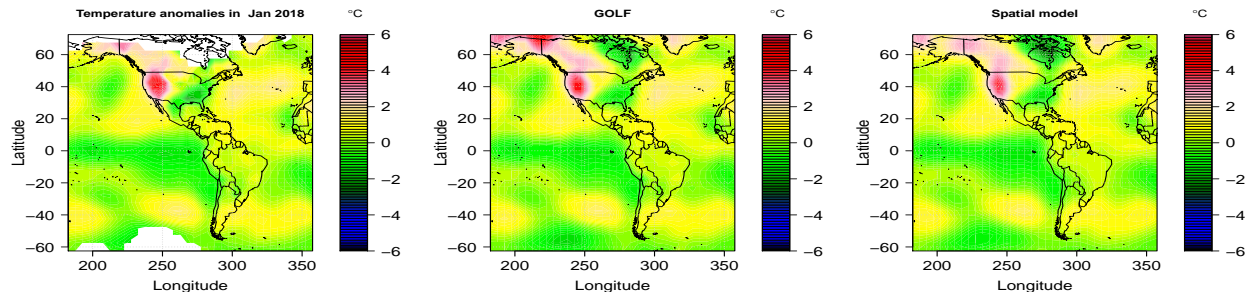


Figure 6: Full temperature anomalies in Jan 2018, predictions by the GOLF model and the spatial model by RobustGaSP package are shown in left, middle and right panels, respectively.

In Table 4, we compare the GOLF processes with a few other spatial and spatio-temporal methods for the NOAA dataset. We fit two spatial models separately for each month using the RobustGaSP package available on CRAN. Also implemented are FRK and LAGP based on their packages (Zammit-Mangion et al., 2017; Gramacy, 2016).

As shown in Table 4, GOLF processes have the smallest predictive RMSE and the shortest predictive interval that covers around 94% of the held-out output. Since the temporal input is not used, it is not surprising that the RMSE and the length of the predictive interval of the two spatial models are larger than the ones by GOLF processes. If we include the temporal inputs, the computation cost is too large for inverting the covariance matrix directly. FRK and LAGP also seem to have a larger predictive error, though both the spatial and temporal inputs are used in these methods.

Predictions from GOLF processes are more accurate due to three reasons. First, we can compute the model with a large number of factors efficiently, and no further approximation of the likelihood function is required. Second, mean and trend parameters at each location are different, making the model flexible to capture the dynamic trend of temperature values at different locations. Finally, Latent factor processes have different kernel parameters that fit diverse smoothness levels of projected observations.

In Figure 6, we graph the full temperature anomalies in Jan 2018, predictions from the GOLF and spatial GP model by RobustGaSP package. 50% of the observation in the left panel are held out for testing. Both models seem to be accurate. Since the temporal coordinate is used in prediction, the predictive error by GOLF processes is smaller.

7 Concluding remarks

We have introduced GOLF processes as a computationally feasible approach to model large incomplete lattice observations. For GPs with a product covariance function or LMC with orthogonal latent factor loadings, the likelihood can be decomposed into a product of multivariate normal densities, and prior independence of factor processes leads to posterior independence of factor processes. These two properties allow one to reduce the computational burden of GPs on incomplete lattice observations without approximating the likelihood function. Further computational reduction can be made by reducing the number of factors as well. Besides, we have introduced a flexible way to model the mean function and the

closed-form marginal likelihood is derived to alleviate the identifiability issue. Finally, we have developed an MCMC algorithm for Bayesian inference for large incomplete matrices of spatial and spatio-temporal data.

The computational tools developed in this work require observations from a lattice with potential missing values. Approximation methods such as the NNGP approach may be integrated to model correlated data with a more general design. Besides, further computational reduction can be made by reducing the number of factors, and a principle way to select the number of factors will be useful. Finally, direct marginalization of factor processes based on an elementwise representation of GPs may be feasible to reduce the computation time from drawing a large number of posterior samples.

Acknowledgements. We thank the editor, associate editor and referee for their comments that substantially improved the article. This research was supported by National Science Foundation under Award Number DMS-2053423 and National Institutes of Health under Award Number R01DK130067. We thank the editor, associate editor and referee for their great suggestions that substantially improve this manuscript.

References

- Anderson, K. R., Johanson, I. A., Patrick, M. R., Gu, M., Segall, P., Poland, M. P., Montgomery-Brown, E. K., and Miklius, A. (2019). Magma reservoir failure and the onset of caldera collapse at kilauea volcano in 2018. *Science*, 366(6470).
- Bai, Z., Demmel, J., Dongarra, J., Ruhe, A., and Vorst, H. v. d. (2000). *Templates for the solution of algebraic eigenvalue problems: a practical guide*. Society for Industrial and Applied Mathematics.
- Banerjee, S., Carlin, B. P., and Gelfand, A. E. (2014). *Hierarchical modeling and analysis for spatial data*. CRC Press.
- Banerjee, S., Gelfand, A. E., Finley, A. O., and Sang, H. (2008). Gaussian predictive process models for large spatial data sets. *Journal of the Royal Statistical Society: Series B (Statistical Methodology)*, 70(4):825–848.
- Bayarri, M. J., Berger, J. O., Paulo, R., Sacks, J., Cafeo, J. A., Cavendish, J., Lin, C.-H., and Tu, J. (2007). A framework for validation of computer models. *Technometrics*, 49(2):138–154.
- Cerbino, R. and Trappe, V. (2008). Differential dynamic microscopy: probing wave vector dependent dynamics with a microscope. *Physical review letters*, 100(18):188102.
- Conti, S. and O’Hagan, A. (2010). Bayesian emulation of complex multi-output and dynamic computer models. *Journal of statistical planning and inference*, 140(3):640–651.
- Cressie, N. and Johannesson, G. (2008). Fixed rank kriging for very large spatial data sets. *Journal of the Royal Statistical Society: Series B (Statistical Methodology)*, 70(1):209–226.

- Cressie, N. A. and Cassie, N. A. (1993). *Statistics for spatial data*. Wiley, New York.
- Datta, A., Banerjee, S., Finley, A. O., and Gelfand, A. E. (2016). Hierarchical nearest-neighbor gaussian process models for large geostatistical datasets. *Journal of the American Statistical Association*, 111(514):800–812.
- Gelfand, A. E., Diggle, P., Guttorp, P., and Fuentes, M. (2010). *Handbook of spatial statistics*. CRC Press.
- Gelfand, A. E., Schmidt, A. M., Banerjee, S., and Sirmans, C. (2004). Nonstationary multivariate process modeling through spatially varying coregionalization. *Test*, 13(2):263–312.
- Gerber, F., Furrer, R., Schaepman-Strub, G., de Jong, R., and Schaepman, M. (2018). Predicting missing values in spatio-temporal satellite data. *IEEE Transactions on Geoscience and Remote Sensing*, 56:2841–2853.
- Gramacy, R. B. (2016). lagp: large-scale spatial modeling via local approximate gaussian processes in r. *Journal of Statistical Software*, 72(1):1–46.
- Gramacy, R. B. and Apley, D. W. (2015). Local Gaussian process approximation for large computer experiments. *Journal of Computational and Graphical Statistics*, 24(2):561–578.
- Gu, M. (2018). Jointly robust prior for Gaussian stochastic process in emulation, calibration and variable selection. *Bayesian Analysis*, 14(1).
- Gu, M. and Shen, W. (2020). Generalized probabilistic principal component analysis of correlated data. *Journal of Machine Learning Research*, 21(13).
- Gu, M. and Xu, Y. (2020). Fast nonseparable Gaussian stochastic process with application to methylation level interpolation. *Journal of Computational and Graphical Statistics*, 29(2):250–260.
- Guinness, J. and Fuentes, M. (2017). Circulant embedding of approximate covariances for inference from gaussian data on large lattices. *Journal of computational and Graphical Statistics*, 26(1):88–97.
- Handcock, M. S. and Stein, M. L. (1993). A bayesian analysis of kriging. *Technometrics*, 35(4):403–410.
- Hartikainen, J. and Sarkka, S. (2010). Kalman filtering and smoothing solutions to temporal gaussian process regression models. In *Machine Learning for Signal Processing (MLSP), 2010 IEEE International Workshop on*, pages 379–384. IEEE.
- Heaton, M. J., Christensen, W. F., and Terres, M. A. (2017). Nonstationary gaussian process models using spatial hierarchical clustering from finite differences. *Technometrics*, 59(1):93–101.

- Heaton, M. J., Datta, A., Finley, A. O., Furrer, R., Guinness, J., Guhaniyogi, R., Gerber, F., Gramacy, R. B., Hammerling, D., Katzfuss, M., et al. (2019). A case study competition among methods for analyzing large spatial data. *Journal of Agricultural, Biological and Environmental Statistics*, 24(3):398–425.
- Higdon, D., Gattiker, J., Williams, B., and Rightley, M. (2008). Computer model calibration using high-dimensional output. *Journal of the American Statistical Association*, 103(482):570–583.
- Katzfuss, M. (2017). A multi-resolution approximation for massive spatial datasets. *Journal of the American Statistical Association*, 112(517):201–214.
- Katzfuss, M. and Guinness, J. (2017). A general framework for vecchia approximations of gaussian processes. *arXiv preprint arXiv:1708.06302*.
- Kaufman, C. G., Schervish, M. J., and Nychka, D. W. (2008). Covariance tapering for likelihood-based estimation in large spatial data sets. *Journal of the American Statistical Association*, 103(484):1545–1555.
- Kennedy, M. C. and O’Hagan, A. (2001). Bayesian calibration of computer models. *Journal of the Royal Statistical Society: Series B (Statistical Methodology)*, 63(3):425–464.
- Kolda, T. G. and Bader, B. W. (2009). Tensor decompositions and applications. *SIAM review*, 51(3):455–500.
- Lindgren, F., Rue, H., and Lindström, J. (2011). An explicit link between gaussian fields and gaussian markov random fields: the stochastic partial differential equation approach. *Journal of the Royal Statistical Society: Series B (Statistical Methodology)*, 73(4):423–498.
- Nychka, D., Bandyopadhyay, S., Hammerling, D., Lindgren, F., and Sain, S. (2015). A multiresolution gaussian process model for the analysis of large spatial datasets. *Journal of Computational and Graphical Statistics*, 24(2):579–599.
- Paulo, R. (2005). Default priors for Gaussian processes. *Annals of statistics*, 33(2):556–582.
- Paulo, R., García-Donato, G., and Palomo, J. (2012). Calibration of computer models with multivariate output. *Computational Statistics and Data Analysis*, 56(12):3959–3974.
- Petris, G., Petrone, S., and Campagnoli, P. (2009). *Dynamic linear models with R*. Springer.
- Rue, H., Martino, S., and Chopin, N. (2009). Approximate bayesian inference for latent gaussian models by using integrated nested laplace approximations. *Journal of the Royal Statistical Society: Series B (Statistical Methodology)*, 71(2):319–392.
- Sacks, J., Welch, W. J., Mitchell, T. J., Wynn, H. P., et al. (1989). Design and analysis of computer experiments. *Statistical science*, 4(4):409–423.
- Särkkä, S. and Hartikainen, J. (2012). Infinite-dimensional kalman filtering approach to spatio-temporal gaussian process regression. In *International Conference on Artificial Intelligence and Statistics*, pages 993–1001.

- Shen, S. S. (2017). *R programming for climate data analysis and visualization: computing and plotting for NOAA data applications*. San Diego State University, USA.
- Sørbye, S. H. and Rue, H. (2011). Simultaneous credible bands for latent gaussian models. *Scandinavian Journal of Statistics*, 38(4):712–725.
- Stein, M. L. (2014). Limitations on low rank approximations for covariance matrices of spatial data. *Spatial Statistics*, 8:1–19.
- Stroud, J. R., Stein, M. L., and Lysen, S. (2017). Bayesian and maximum likelihood estimation for gaussian processes on an incomplete lattice. *Journal of computational and Graphical Statistics*, 26(1):108–120.
- Teh, Y. W., Seeger, M., and Jordan, M. I. (2005). Semiparametric latent factor models. In Cowell, R. G. and Ghahramani, Z., editors, *Proceedings of the Tenth International Workshop on Artificial Intelligence and Statistics*, volume R5 of *Proceedings of Machine Learning Research*, pages 333–340. PMLR.
- Tipping, M. E. and Bishop, C. M. (1999). Probabilistic principal component analysis. *Journal of the Royal Statistical Society: Series B (Statistical Methodology)*, 61(3):611–622.
- Vecchia, A. V. (1988). Estimation and model identification for continuous spatial processes. *Journal of the Royal Statistical Society: Series B (Methodological)*, 50(2):297–312.
- West, M. and Harrison, P. J. (1997). *Bayesian Forecasting & Dynamic Models*. Springer Verlag, 2nd edition.
- Whittle, P. (1963). Stochastic process in several dimensions. *Bulletin of the International Statistical Institute*, 40(2):974–994.
- Zammit-Mangion, Andrew, and Cressie, N. (2017). Frk: An r package for spatial and spatio-temporal prediction with large datasets. *arXiv preprint arXiv:1106.6251*.
- Zimmerman, D. L. (1993). Another look at anisotropy in geostatistics. *Mathematical Geology*, 25(4):453–470.

Supplementary materials

This supplementary materials contain three parts. The proof of Section 2 is given in Section S1. The additional numerical results for the simulated studies and real applications are given in Section S2 and Section S3, respectively.

S1 Proofs for Section 2

S1.1 Auxiliary facts

1. Let \mathbf{A} and \mathbf{B} be matrices,

$$(\mathbf{A} \otimes \mathbf{B})^T = (\mathbf{A}^T \otimes \mathbf{B}^T);$$

further assuming \mathbf{A} and \mathbf{B} are invertible,

$$(\mathbf{A} \otimes \mathbf{B})^{-1} = \mathbf{A}^{-1} \otimes \mathbf{B}^{-1}.$$

2. Let \mathbf{A} , \mathbf{B} , \mathbf{C} and \mathbf{D} be the matrices such that the products \mathbf{AC} and \mathbf{BD} are matrices,

$$(\mathbf{A} \otimes \mathbf{B})(\mathbf{C} \otimes \mathbf{D}) = (\mathbf{AC}) \otimes (\mathbf{BD}).$$

3. For matrices \mathbf{A} , \mathbf{B} and \mathbf{C} ,

$$(\mathbf{C}^T \otimes \mathbf{A})\text{vec}(\mathbf{B}) = \text{vec}(\mathbf{ABC});$$

further assuming $\mathbf{A}^T\mathbf{B}$ is a matrix,

$$\text{tr}(\mathbf{A}^T\mathbf{B}) = \text{vec}(\mathbf{A})^T\text{vec}(\mathbf{B}).$$

4. For any invertible $n \times n$ matrix \mathbf{C} ,

$$|\mathbf{C} + \mathbf{AB}| = |\mathbf{C}||\mathbf{I}_n + \mathbf{BC}^{-1}\mathbf{A}|.$$

S1.2 Proofs for Section 2.1

The following denotation are used in the proof: $\mathbf{Y}_{-M} = \mathbf{Y} - \mathbf{M}$, $\mathbf{Y}_{v,-M} = \text{vec}(\mathbf{Y} - \mathbf{M})$, $\mathbf{Z}_{vt} = \text{vec}(\mathbf{Z}^T)$ and $\mathbf{A}_v = [\mathbf{I}_{n_2} \otimes \mathbf{a}_1, \dots, \mathbf{I}_{n_2} \otimes \mathbf{a}_d]$. Let $\mathbf{\Sigma}_v$ be an $n_2d \times n_2d$ matrix where the l th diagonal block is $\mathbf{\Sigma}_l$. Denote $\text{etr}(\cdot) = \exp(\text{tr}(\cdot))$.

Proof of Equation 4. Denote $C_Y = (2\pi\sigma_0^2)^{-\frac{n_1 n_2}{2}} \prod_{l=1}^d |\Sigma_l/\sigma_0^2 + \mathbf{I}_{n_2}|^{-1/2}$. Directly marginalizing out \mathbf{Z} , one has

$$\begin{aligned}
& p(\mathbf{Y} \mid \Theta) \\
&= C_Y \exp \left(-\frac{\mathbf{Y}_{v,-M}^T \left(\mathbf{I}_{n_1 n_2} - \sum_{l=1}^d (\sigma_0^2 \Sigma_l^{-1} + \mathbf{I}_{n_2})^{-1} \otimes (\mathbf{a}_l \mathbf{a}_l^T) \right) \mathbf{Y}_{v,-M}}{2\sigma_0^2} \right) \\
&= C_Y \exp \left(-\frac{\mathbf{Y}_{v,-M}^T \mathbf{Y}_{v,-M} - \mathbf{Y}_{v,-M}^T \sum_{l=1}^d \text{vec}(\mathbf{a}_l \mathbf{a}_l^T \mathbf{Y}_{v,-M} (\sigma_0^2 \Sigma_l^{-1} + \mathbf{I}_{n_2})^{-1})}{2\sigma_0^2} \right) \\
&= C_Y \text{etr} \left(-\frac{\mathbf{Y}_{-M}^T \mathbf{Y}_{-M} - \sum_{l=1}^d \tilde{\mathbf{y}}_l \tilde{\mathbf{y}}_l^T (\sigma_0^2 \Sigma_l^{-1} + \mathbf{I}_{n_2})^{-1}}{2\sigma_0^2} \right) \\
&= C_Y \exp \left(-\frac{\sum_{l=1}^d \tilde{\mathbf{y}}_l^T (\Sigma_l/\sigma_0^2 + \mathbf{I}_{n_2})^{-1} \tilde{\mathbf{y}}_l + \sum_{l=d+1}^{n_1} \tilde{\mathbf{y}}_l^T \tilde{\mathbf{y}}_l}{2\sigma_0^2} \right),
\end{aligned}$$

where the first equation is based on Lemma 1 and the Woodbury matrix identity (to compute the normalizing constant C_Y); the second and third equations are from fact 3; the fourth equation is from Woodbury matrix identity. The Equation (4) follows immediately. \square

Proof of Corollary 1. The proof is implied by the proof of Theorem 4 in (Gu and Shen, 2020). For completeness of this article, we include the proof below.

From Equation (1) and Equation (2), we have

$$\begin{aligned}
p(\mathbf{Z}_{vt} \mid \mathbf{Y}, \Theta) &\propto \exp \left(\frac{(\mathbf{Y}_{v,-M} - \mathbf{A}_v \mathbf{Z}_{vt})^T (\mathbf{Y}_{v,-M} - \mathbf{A}_v \mathbf{Z}_{vt})}{2\sigma_0^2} \right) \exp \left(-\frac{1}{2} \mathbf{Z}_{vt}^T \Sigma_v^{-1} \mathbf{Z}_{vt} \right) \\
&\propto \exp \left\{ -\frac{1}{2} (\mathbf{Z}_{vt} - \boldsymbol{\mu}_{Z_{vt}})^T \left(\frac{\mathbf{A}_v^T \mathbf{A}_v}{\sigma_0^2} + \Sigma_v^{-1} \right) (\mathbf{Z}_{vt} - \boldsymbol{\mu}_{Z_{vt}}) \right\},
\end{aligned}$$

where $\boldsymbol{\mu}_{Z_{vt}} = (\mathbf{A}_v^T \mathbf{A}_v + \sigma_0^2 \Sigma_v^{-1})^{-1} \mathbf{A}_v^T \mathbf{Y}_{v,-M}$. Note $\mathbf{A}_v^T \mathbf{A}_v = \mathbf{I}_{n_2 d}$, from which we have

$$\mathbf{Z}_{vt} \mid \mathbf{Y}, \Theta \sim \text{MN} \left(\boldsymbol{\mu}_{Z_{vt}}, \left(\frac{1}{\sigma_0^2} \mathbf{I}_{n_2 d} + \Sigma_v^{-1} \right)^{-1} \right). \quad (\text{S1})$$

Based on vectorization, one has

$$\begin{aligned}
\boldsymbol{\mu}_{Z_{vt}} &= \begin{pmatrix} (\sigma_0^2 \Sigma_1^{-1} + \mathbf{I}_{n_2})^{-1} \otimes \mathbf{a}_1^T \\ \vdots \\ (\sigma_0^2 \Sigma_d^{-1} + \mathbf{I}_{n_2})^{-1} \otimes \mathbf{a}_d^T \end{pmatrix} \text{vec}(\mathbf{Y}) = \begin{pmatrix} \text{vec} \left(\mathbf{a}_1^T \mathbf{Y}_{-M} (\sigma_0^2 \Sigma_1^{-1} + \mathbf{I}_{n_2})^{-1} \right) \\ \vdots \\ \text{vec} \left(\mathbf{a}_d^T \mathbf{Y}_{-M} (\sigma_0^2 \Sigma_d^{-1} + \mathbf{I}_{n_2})^{-1} \right) \end{pmatrix} \\
&= \text{vec} \left(\begin{pmatrix} \mathbf{a}_1^T \mathbf{Y}_{-M} (\sigma_0^2 \Sigma_1^{-1} + \mathbf{I}_{n_2})^{-1} \\ \vdots \\ \mathbf{a}_d^T \mathbf{Y}_{-M} (\sigma_0^2 \Sigma_d^{-1} + \mathbf{I}_{n_2})^{-1} \end{pmatrix}^T \right). \quad (\text{S2})
\end{aligned}$$

Note that the covariance matrix of $\boldsymbol{\mu}_{Z_{vt}}$ is a block diagonal matrix. The results follow by Equation (S2) and the Woodbury matrix identity. \square

S1.3 Proofs for Section 2.2

Note $\mathbf{A}_F = [\mathbf{A}_s, \mathbf{A}_c] = [\mathbf{a}_1, \mathbf{a}_2, \dots, \mathbf{a}_{n_1}]$, where \mathbf{A}_c is an $n_1 \times (n_1 - d)$ matrix of the orthogonal complement of \mathbf{A}_s . We need the following lemma to prove Theorem 1.

Lemma S1. *After marginalizing out the factors \mathbf{Z} , we have the marginal posterior distribution of the transformed regression coefficients,*

1. *(Marginal distribution of transformed row regression coefficients). Assume $\mathbf{M} = \mathbf{H}_1 \mathbf{B}_1$ and the objective prior $\pi(\mathbf{B}_1) \propto 1$ for \mathbf{B}_1 . Let $\tilde{\mathbf{B}}_1 = [\tilde{\mathbf{b}}_{1,1}, \dots, \tilde{\mathbf{b}}_{1,n_1}] = \mathbf{B}_1^T \mathbf{H}_1^T \mathbf{A}_F$ be an $n_2 \times n_1$ matrix of transformed coefficients. Assume the marginal posterior distribution of $\tilde{\mathbf{B}}_1$ follows*

$$p(\tilde{\mathbf{B}}_1 \mid \mathbf{Y}, \boldsymbol{\Theta}_{-B_1}) = \prod_{l=1}^d \mathcal{PN}(\tilde{\mathbf{b}}_{1,l}; \tilde{\mathbf{y}}_l, \tilde{\boldsymbol{\Sigma}}_l) \prod_{l=d+1}^{n_1} \mathcal{PN}(\tilde{\mathbf{b}}_{1,l}; \tilde{\mathbf{y}}_l, \sigma_0^2 \mathbf{I}_{n_2}), \quad (\text{S3})$$

where $\tilde{\mathbf{y}}_l$ is defined in equation (4) and $\tilde{\boldsymbol{\Sigma}}_l$ is defined in corollary 1. Then we can sample $(\mathbf{B}_1 \mid \mathbf{Y}, \boldsymbol{\Theta}_{-B_1})$ by $(\mathbf{H}_1^T \mathbf{H}_1)^{-1} \mathbf{H}_1^T \mathbf{A}_F \tilde{\mathbf{B}}_1^T$, where $\tilde{\mathbf{B}}_1^T$ are sampled from the $p(\tilde{\mathbf{B}}_1 \mid \mathbf{Y}, \boldsymbol{\Theta}_{-B_1})$ in equation (S3).

2. *(Marginal distribution of transformed column regression coefficients). Assume $\mathbf{M} = (\mathbf{H}_2 \mathbf{B}_2)^T$ and the objective prior $\pi(\mathbf{B}_2) \propto 1$ for the regression parameters \mathbf{B}_2 . Let $\tilde{\mathbf{B}}_2 = [\tilde{\mathbf{b}}_{2,1}, \dots, \tilde{\mathbf{b}}_{2,n_1}] = \mathbf{B}_2 \mathbf{A}_F$ be a $q_2 \times n_1$ matrix. The marginal posterior distribution of $\tilde{\mathbf{B}}_2$ follows*

$$p(\tilde{\mathbf{B}}_2 \mid \mathbf{Y}, \boldsymbol{\Theta}_{-B_2}) = \prod_{l=1}^{n_1} \mathcal{PN}(\tilde{\mathbf{b}}_{2,l}; \boldsymbol{\mu}_{\tilde{\mathbf{b}}_{2,l}}, \boldsymbol{\Sigma}_{\tilde{\mathbf{b}}_{2,l}}), \quad (\text{S4})$$

where $\boldsymbol{\mu}_{\tilde{\mathbf{b}}_{2,l}} = (\mathbf{H}_2^T \tilde{\boldsymbol{\Sigma}}_l^{-1} \mathbf{H}_2)^{-1} \mathbf{H}_2^T \tilde{\boldsymbol{\Sigma}}_l^{-1} \tilde{\mathbf{y}}_l$ and $\boldsymbol{\Sigma}_{\tilde{\mathbf{b}}_{2,l}} = (\mathbf{H}_2^T \tilde{\boldsymbol{\Sigma}}_l^{-1} \mathbf{H}_2)^{-1}$ for $l = 1, \dots, d$; $\boldsymbol{\mu}_{\tilde{\mathbf{b}}_{2,l}} = (\mathbf{H}_2^T \mathbf{H}_2)^{-1} \mathbf{H}_2^T \tilde{\mathbf{y}}_l$ and $\boldsymbol{\Sigma}_{\tilde{\mathbf{b}}_{2,l}} = \sigma_0^2 (\mathbf{H}_2^T \mathbf{H}_2)^{-1}$ for $l = d+1, \dots, n_1$.

Proof of Lemma S1. 1. (Marginal distribution of transformed row regression coefficients).

Denote $(\mathbf{B}_1^{aug}) = [\mathbf{B}_1^T, \tilde{\mathbf{B}}_{1,(q_1+1):n_1}]^T$, where $\tilde{\mathbf{B}}_{1,(q_1+1):n_1}$ are the last $n_1 - q_1$ columns of $\tilde{\mathbf{B}}_1$. Denote $p_{trans}(\mathbf{B}_1 \mid \mathbf{Y}, \boldsymbol{\Theta}_{-B_1})$ and $p_{trans}(\mathbf{B}_1^{aug} \mid \mathbf{Y}, \boldsymbol{\Theta}_{-B_1})$ the transformed marginal posterior distribution of \mathbf{B}_1 and \mathbf{B}_1^{aug} derived by transforming $p(\tilde{\mathbf{B}}_1 \mid \mathbf{Y}, \boldsymbol{\Theta}_{-B_1})$ in (S3).

We have

$$\begin{aligned}
p_{trans}(\mathbf{B}_1 \mid \mathbf{Y}, \boldsymbol{\Theta}_{-\mathbf{B}_1}) &\propto p_{trans}(\mathbf{B}_1^{aug} \mid \mathbf{Y}, \boldsymbol{\Theta}_{-\mathbf{B}_1}) = p(\tilde{\mathbf{B}}_1 \mid \mathbf{Y}, \boldsymbol{\Theta}_{-\mathbf{B}_1}) \left| \frac{d\tilde{\mathbf{B}}_1}{d\mathbf{B}_1^{aug}} \right| \\
&\propto \exp \left\{ -\frac{1}{2} \sum_{l=1}^d (\tilde{\mathbf{b}}_{1,l} - \tilde{\mathbf{y}}_l)^T \tilde{\boldsymbol{\Sigma}}_l^{-1} (\tilde{\mathbf{b}}_{1,l} - \tilde{\mathbf{y}}_l) - \frac{1}{2\sigma_0^2} \sum_{l=d+1}^{n_1} (\tilde{\mathbf{b}}_{1,l} - \tilde{\mathbf{y}}_l)^T (\tilde{\mathbf{b}}_{1,l} - \tilde{\mathbf{y}}_l) \right\} \\
&\propto \exp \left\{ -\frac{1}{2} \sum_{l=1}^d \mathbf{a}_l^T (\mathbf{Y} - \mathbf{H}_1 \mathbf{B}_1) \tilde{\boldsymbol{\Sigma}}_l^{-1} (\mathbf{Y} - \mathbf{H}_1 \mathbf{B}_1)^T \mathbf{a}_l \right. \\
&\quad \left. - \frac{1}{2\sigma_0^2} \sum_{l=d+1}^{n_1} \mathbf{a}_l^T (\mathbf{Y} - \mathbf{H}_1 \mathbf{B}_1) (\mathbf{Y} - \mathbf{H}_1 \mathbf{B}_1)^T \mathbf{a}_l \right\},
\end{aligned}$$

where the last line is the same as the posterior distribution of \mathbf{B}_1 based on the marginal likelihood in equation (4) and the prior distribution $\pi(\mathbf{B}_1) \propto 1$. Thus if one sample $\tilde{\mathbf{B}}_1$ from (S3), one can obtain the sample for $(\mathbf{B}_1 \mid \mathbf{Y}, \boldsymbol{\Theta}_{-\mathbf{B}_1})$ through $(\mathbf{H}_1^T \mathbf{H}_1)^{-1} \mathbf{H}_1^T \mathbf{A}_F \tilde{\mathbf{B}}_1^T$.

2. (Marginal distribution of transformed column regression coefficients).

Since $\pi(\mathbf{B}_2) \propto 1$ is a Jeffreys prior, and $\tilde{\mathbf{B}}_2$ is a linear transformation of \mathbf{B}_2 with the same dimension, we have $\pi(\tilde{\mathbf{B}}_2) \propto 1$.

Based on the marginal likelihood in equation (4) and the prior distribution, the posterior distribution of $\tilde{\mathbf{B}}_2$ follows:

$$\begin{aligned}
&p(\tilde{\mathbf{B}}_2 \mid \mathbf{Y}, \boldsymbol{\Theta}_{-\mathbf{B}_2}) \\
&\propto \exp \left\{ -\frac{1}{2} \sum_{l=1}^d \mathbf{a}_l^T (\mathbf{Y} - \mathbf{B}_2^T \mathbf{H}_2^T) \tilde{\boldsymbol{\Sigma}}_l^{-1} (\mathbf{Y} - \mathbf{B}_2^T \mathbf{H}_2^T)^T \mathbf{a}_l \right. \\
&\quad \left. - \frac{1}{2\sigma_0^2} \sum_{l=d+1}^{n_1} \mathbf{a}_l^T (\mathbf{Y} - \mathbf{B}_2^T \mathbf{H}_2^T) (\mathbf{Y} - \mathbf{B}_2^T \mathbf{H}_2^T)^T \mathbf{a}_l \right\} \\
&\propto \exp \left\{ -\frac{1}{2} \sum_{l=1}^d (\tilde{\mathbf{y}}_l - \mathbf{H}_2 \tilde{\mathbf{b}}_{2,l})^T \tilde{\boldsymbol{\Sigma}}_l^{-1} (\tilde{\mathbf{y}}_l - \mathbf{H}_2 \tilde{\mathbf{b}}_{2,l}) \right. \\
&\quad \left. - \frac{1}{2\sigma_0^2} \sum_{l=d+1}^{n_1} (\tilde{\mathbf{y}}_l - \mathbf{H}_2 \tilde{\mathbf{b}}_{2,l})^T (\tilde{\mathbf{y}}_l - \mathbf{H}_2 \tilde{\mathbf{b}}_{2,l}) \right\} \\
&\propto \exp \left\{ -\frac{1}{2} \sum_{l=1}^d \left(\tilde{\mathbf{b}}_{2,l} - \boldsymbol{\mu}_{\tilde{\mathbf{b}}_{2,l}} \right)^T \mathbf{H}_2^T \tilde{\boldsymbol{\Sigma}}_l^{-1} \mathbf{H}_2 \left(\tilde{\mathbf{b}}_{2,l} - \boldsymbol{\mu}_{\tilde{\mathbf{b}}_{2,l}} \right) \right. \\
&\quad \left. - \frac{1}{2\sigma_0^2} \sum_{l=d+1}^{n_1} \left(\tilde{\mathbf{b}}_{2,l} - \boldsymbol{\mu}_{\tilde{\mathbf{b}}_{2,l}} \right)^T \mathbf{H}_2^T \mathbf{H}_2 \left(\tilde{\mathbf{b}}_{2,l} - \boldsymbol{\mu}_{\tilde{\mathbf{b}}_{2,l}} \right) \right\},
\end{aligned}$$

from which equation (S4) follows. □

We are ready to prove Theorem 1.

Proof of Theorem 1. After marginalizing out \mathbf{Z} , we have

1. (Row regression coefficients).

From Lemma S1, the posterior mean of $(\tilde{\mathbf{B}}_1 \mid \mathbf{Y}, \boldsymbol{\Theta}_{-\mathbf{B}_1})$ is $\mathbf{Y}^T \mathbf{A}_F$, where $\mathbf{A}_F := [\mathbf{A}_s, \mathbf{A}_c]$. We denote the centered $\tilde{\mathbf{B}}_1$ by $\tilde{\mathbf{B}}_{1,0} = [\tilde{\mathbf{B}}_{1,0,s}, \tilde{\mathbf{B}}_{1,0,c}] = \tilde{\mathbf{B}}_1 - \mathbf{Y}^T \mathbf{A}_F$, where $\tilde{\mathbf{B}}_{1,0,s}$ is the first d columns of $\tilde{\mathbf{B}}_{1,0}$ and $\tilde{\mathbf{B}}_{1,0,c}$ is the last $(n_1 - d)$ columns of $\tilde{\mathbf{B}}_{1,0}$. Let $\tilde{\mathbf{b}}_{1,0,l}$ be the l -th column of $\tilde{\mathbf{B}}_{1,0}$. Then the posterior mean of $(\mathbf{B}_1 \mid \mathbf{Y}, \boldsymbol{\Theta}_{-\mathbf{B}_1})$ can be calculated below

$$\begin{aligned} \hat{\mathbf{B}}_1 &= \mathbb{E}(\mathbf{B}_1 \mid \mathbf{Y}, \boldsymbol{\Theta}_{-\mathbf{B}_1}) = \mathbb{E} \left((\mathbf{H}_1^T \mathbf{H}_1)^{-1} \mathbf{H}_1^T \mathbf{A}_F \tilde{\mathbf{B}}_1^T \mid \mathbf{Y}, \boldsymbol{\Theta}_{-\mathbf{B}_1} \right) \\ &= (\mathbf{H}_1^T \mathbf{H}_1)^{-1} \mathbf{H}_1^T \mathbf{A}_F \mathbf{A}_F^T \mathbf{Y} = (\mathbf{H}_1^T \mathbf{H}_1)^{-1} \mathbf{H}_1^T \mathbf{Y} \end{aligned}$$

Note $\mathbf{B}_1 = (\mathbf{H}_1^T \mathbf{H}_1)^{-1} \mathbf{H}_1^T \mathbf{A}_F \tilde{\mathbf{B}}_1^T$, one has

$$\mathbf{B}_1 - \hat{\mathbf{B}}_1 = (\mathbf{H}_1^T \mathbf{H}_1)^{-1} \mathbf{H}_1^T \mathbf{A}_F (\tilde{\mathbf{B}}_{1,0})^T = (\mathbf{H}_1^T \mathbf{H}_1)^{-1} \mathbf{H}_1^T \left(\mathbf{A}_s \tilde{\mathbf{B}}_{1,0,s}^T + \mathbf{A}_c \tilde{\mathbf{B}}_{1,0,c}^T \right)$$

where $\tilde{\mathbf{B}}_{1,0,s}$ is a $n_2 \times d$ matrix with the l th column independently sampled from $\mathcal{N}(\mathbf{0}, \tilde{\boldsymbol{\Sigma}}_l)$ for $l = 1, \dots, d$. For the distribution of $\mathbf{A}_c \tilde{\mathbf{B}}_{1,0,c}^T$, using part 1 of Lemma S1, we have

$$\begin{aligned} p(\mathbf{A}_c \tilde{\mathbf{B}}_{1,0,c}^T \mid \mathbf{Y}, \boldsymbol{\Theta}_{-\mathbf{B}_1}) &\propto \exp \left\{ -\frac{1}{2\sigma_0^2} \text{tr} \left(\mathbf{A}_c^T \tilde{\mathbf{B}}_{1,0,c} \tilde{\mathbf{B}}_{1,0,c}^T \mathbf{A}_c \right) \right\} \\ &\propto \exp \left\{ -\frac{1}{2\sigma_0^2} \text{tr} \left((\mathbf{I}_{n_1} - \mathbf{A}_s \mathbf{A}_s^T) \tilde{\mathbf{B}}_{1,0,c} \tilde{\mathbf{B}}_{1,0,c}^T \right) \right\}. \end{aligned}$$

Thus we can sample $\mathbf{A}_c \tilde{\mathbf{B}}_{1,0,c}^T$ by $\sigma_0 (\mathbf{I}_{n_1} - \mathbf{A}_s \mathbf{A}_s^T) \mathbf{Z}_{0,1}$, where $\mathbf{Z}_{0,1}$ is an $n_1 \times n_2$ matrix with each entry independently sampled from standard normal distribution. The results soon follow.

2. (Column regression coefficients).

We first compute the posterior mean of $(\mathbf{B}_2 \mid \mathbf{Y}, \boldsymbol{\Theta}_{-\mathbf{B}_2})$ below

$$\begin{aligned} \hat{\mathbf{B}}_2 &= \mathbb{E}(\mathbf{B}_2 \mid \mathbf{Y}, \boldsymbol{\Theta}_{-\mathbf{B}_2}) = \mathbb{E}(\tilde{\mathbf{B}}_2 \mathbf{A}_F^T \mid \mathbf{Y}, \boldsymbol{\Theta}_{-\mathbf{B}_2}) \\ &= \sum_{l=1}^d (\mathbf{H}_2^T \tilde{\boldsymbol{\Sigma}}_l^{-1} \mathbf{H}_2)^{-1} \mathbf{H}_2^T \tilde{\boldsymbol{\Sigma}}_l^{-1} \mathbf{Y}^T \mathbf{a}_l \mathbf{a}_l^T + (\mathbf{H}_2^T \mathbf{H}_2)^{-1} \mathbf{H}_2^T \mathbf{Y}^T (\mathbf{I}_{n_1} - \mathbf{A}_s \mathbf{A}_s^T) \end{aligned}$$

We denote the centered $\tilde{\mathbf{B}}_2$ by $\tilde{\mathbf{B}}_{2,0} = [\tilde{\mathbf{B}}_{2,0,s}, \tilde{\mathbf{B}}_{2,0,c}]$. We have

$$\mathbf{B}_2 - \hat{\mathbf{B}}_2 = \tilde{\mathbf{B}}_{2,0} \mathbf{A}_F^T = \tilde{\mathbf{B}}_{2,0,s} \mathbf{A}_s^T + \tilde{\mathbf{B}}_{2,0,c} \mathbf{A}_c^T$$

where $\tilde{\mathbf{B}}_{2,0,s}$ is a $q_2 \times d$ matrix with the l th column independently sampled from $\mathcal{N}(\mathbf{0}, (\mathbf{H}_2^T \tilde{\Sigma}_l^{-1} \mathbf{H}_2)^{-1})$ for $l = 1, \dots, d$. For the distribution of $\tilde{\mathbf{B}}_{2,0,c} \mathbf{A}_c^T$, we have

$$\begin{aligned} p(\tilde{\mathbf{B}}_{2,0,c} \mathbf{A}_c^T \mid \mathbf{Y}, \boldsymbol{\Theta}_{-\mathbf{B}_2}) &\propto \exp \left\{ -\frac{1}{2\sigma_0^2} \text{tr} \left(\mathbf{A}_c \mathbf{A}_c^T \tilde{\mathbf{B}}_{2,0,c} \mathbf{H}_2^T \mathbf{H}_2 \tilde{\mathbf{B}}_{2,0,c}^T \right) \right\} \\ &\propto \exp \left\{ -\frac{1}{2\sigma_0^2} \text{tr} \left((\mathbf{I}_{n_1} - \mathbf{A}_s \mathbf{A}_s^T) \tilde{\mathbf{B}}_{2,0,c} \mathbf{H}_2^T \mathbf{H}_2 \tilde{\mathbf{B}}_{2,0,c}^T \right) \right\}. \end{aligned}$$

Thus we can sample $\tilde{\mathbf{B}}_{2,0,c} \mathbf{A}_c^T$ by $\sigma_0(\mathbf{I}_{n_1} - \mathbf{A}_s \mathbf{A}_s^T) \mathbf{Z}_{0,2}^T \mathbf{L}_{H_2}^T$, where \mathbf{L}_{H_2} is a $q_2 \times q_2$ matrix such that $\mathbf{L}_{H_2} \mathbf{L}_{H_2}^T = (\mathbf{H}_2^T \mathbf{H}_2)^{-1}$ and $\mathbf{Z}_{0,2}$ is a $q_2 \times n_1$ matrix with each entry independently sampled from standard normal distribution.

□

Lemma S2. Assume $\mathbf{M} = \mathbf{H}_1 \mathbf{B}_1 + (\mathbf{H}_2 \mathbf{B}_2)^T$ and let the objective prior $\pi(\mathbf{B}_1, \mathbf{B}_2) \propto 1$ for the regression parameters \mathbf{B}_1 and \mathbf{B}_2 . Denote $\tilde{\mathbf{B}}_1 = [\tilde{\mathbf{b}}_{1,1}, \dots, \tilde{\mathbf{b}}_{1,n_1}] = \mathbf{B}_1^T \mathbf{H}_1^T \mathbf{A}_F$ and $\tilde{\mathbf{B}}_2 = [\tilde{\mathbf{b}}_{2,1}, \dots, \tilde{\mathbf{b}}_{2,n_1}] = \mathbf{B}_2 \mathbf{A}_F$.

1. After marginalizing out \mathbf{Z} and \mathbf{B}_1 , assume the marginal posterior distribution of $\tilde{\mathbf{B}}_1$ follows

$$p(\tilde{\mathbf{B}}_1 \mid \mathbf{Y}, \boldsymbol{\Theta}_{-\mathbf{B}_1, -\mathbf{B}_2}) = \prod_{l=1}^{n_1} \mathcal{PN}(\tilde{\mathbf{b}}_{1,l}; \tilde{\mathbf{y}}_l, \mathbf{Q}_{1,l}). \quad (\text{S5})$$

where $\mathbf{Q}_{1,l} = \mathbf{P}_l^T (\tilde{\Sigma}_l)^{-1} \mathbf{P}_l$, $\mathbf{P}_l = \mathbf{I}_{n_2} - \mathbf{H}_2 (\mathbf{H}_2^T \tilde{\Sigma}_l^{-1} \mathbf{H}_2)^{-1} \mathbf{H}_2^T \tilde{\Sigma}_l^{-1}$ for $l = 1, \dots, d$ and $\mathbf{Q}_{1,l} = \sigma_0^2 \mathbf{P}_0$ with $\mathbf{P}_0 = (\mathbf{I}_{n_2} - \mathbf{H}_2 (\mathbf{H}_2^T \mathbf{H}_2)^{-1} \mathbf{H}_2^T)$ for $l = d+1, \dots, n_1$. The sample $(\mathbf{B}_1 \mid \mathbf{Y}, \boldsymbol{\Theta}_{-\mathbf{B}_1, -\mathbf{B}_2})$ can be obtained by $(\mathbf{H}_1^T \mathbf{H}_1)^{-1} \mathbf{H}_1^T \mathbf{A}_F \tilde{\mathbf{B}}_1^T$, where $\tilde{\mathbf{B}}_1$ sampled from the $p(\tilde{\mathbf{B}}_1 \mid \mathbf{Y}, \boldsymbol{\Theta}_{-\mathbf{B}_1, -\mathbf{B}_2})$ in equation (S5).

2. After marginalizing out \mathbf{Z} and conditional on \mathbf{B}_1 , the marginal posterior distribution of $\tilde{\mathbf{B}}_2$ follows (S4) by replacing $\tilde{\mathbf{y}}_l$ by $\tilde{\mathbf{y}}_{l,B_1} = (\mathbf{Y} - \mathbf{H}_1 \mathbf{B}_1)^T \mathbf{a}_l$ for $l = 1, \dots, d$.

Proof of Lemma S2. Denote $\mathbf{Y}_0 = \mathbf{Y} - \mathbf{H}_1 \mathbf{B}_1 - \mathbf{B}_2^T \mathbf{H}_2^T$. Define $\mathbf{G} = [\mathbf{g}_1, \mathbf{g}_2, \dots, \mathbf{g}_{n_1}] = (\mathbf{Y} - \mathbf{H}_1 \mathbf{B}_1)^T \mathbf{A}_F$. That is, $\mathbf{g}_l = (\mathbf{Y} - \mathbf{H}_1 \mathbf{B}_1)^T \mathbf{a}_l$.

First we have the joint posterior distribution $(\mathbf{B}_1, \mathbf{B}_2 \mid \mathbf{Y}, \boldsymbol{\Theta}_{-\mathbf{B}_1, -\mathbf{B}_2})$

$$\begin{aligned} &p(\mathbf{B}_1, \mathbf{B}_2 \mid \mathbf{Y}, \boldsymbol{\Theta}_{-\mathbf{B}_1, -\mathbf{B}_2}) \\ &\propto \exp \left\{ -\frac{1}{2} \sum_{l=1}^d \mathbf{a}_l^T \mathbf{Y}_0^T \tilde{\Sigma}_l^{-1} \mathbf{Y}_0 \mathbf{a}_l - \frac{1}{2\sigma_0^2} \sum_{l=d+1}^{n_1} \mathbf{a}_l^T \mathbf{Y}_0^T \mathbf{Y}_0 \mathbf{a}_l \right\} \\ &\propto \exp \left\{ -\frac{1}{2} \sum_{l=1}^d (\mathbf{g}_l - \mathbf{H}_2 \tilde{\mathbf{b}}_{2,l})^T \tilde{\Sigma}_l^{-1} (\mathbf{g}_l - \mathbf{H}_2 \tilde{\mathbf{b}}_{2,l}) - \frac{1}{2\sigma_0^2} \sum_{l=d+1}^{n_1} (\mathbf{g}_l - \mathbf{H}_2 \tilde{\mathbf{b}}_{2,l})^T (\mathbf{g}_l - \mathbf{H}_2 \tilde{\mathbf{b}}_{2,l}) \right\}, \end{aligned}$$

where $\tilde{\mathbf{b}}_{2,l}$ is a transformation of \mathbf{B}_2 defined in part 2 in Lemma S1.

After integrating out $\tilde{\mathbf{b}}_{2,l}$ from $p(\mathbf{B}_1, \mathbf{B}_2 \mid \mathbf{Y}, \boldsymbol{\Theta}_{-\mathbf{B}_1, -\mathbf{B}_2})$ for $l = 1, 2, \dots, n_1$, one has

$$\begin{aligned}
& p(\mathbf{B}_1 \mid \mathbf{Y}, \boldsymbol{\Theta}_{-\mathbf{B}_1, -\mathbf{B}_2}) \\
& \propto \exp \left\{ -\frac{\sum_{l=1}^d (\mathbf{g}_l - \mathbf{H}_2 \hat{\mathbf{b}}_{2,l})^T \tilde{\boldsymbol{\Sigma}}_l^{-1} (\mathbf{g}_l - \mathbf{H}_2 \hat{\mathbf{b}}_{2,l})}{2} - \frac{\sum_{l=d+1}^{n_1} (\mathbf{g}_l - \mathbf{H}_2 \hat{\mathbf{b}}_{2,l})^T (\mathbf{g}_l - \mathbf{H}_2 \hat{\mathbf{b}}_{2,l})}{2\sigma_0^2} \right\} \\
& \propto \exp \left\{ -\frac{\sum_{l=1}^d \mathbf{g}_l^T \mathbf{P}_l^T (\tilde{\boldsymbol{\Sigma}}_l)^{-1} \mathbf{P}_l \mathbf{g}_l}{2} - \frac{\sum_{l=d+1}^{n_1} \mathbf{g}_l^T \mathbf{P}_0 \mathbf{g}_l}{2\sigma_0^2} \right\} \\
& \propto \exp \left\{ -\frac{\sum_{l=1}^{n_1} \mathbf{g}_l^T \mathbf{Q}_{1,l} \mathbf{g}_l}{2} \right\}
\end{aligned}$$

Where

$$\hat{\mathbf{b}}_{2,l} = \begin{cases} (\mathbf{H}_2^T \tilde{\boldsymbol{\Sigma}}_l^{-1} \mathbf{H}_2)^{-1} \mathbf{H}_2^T \tilde{\boldsymbol{\Sigma}}_l^{-1} \mathbf{g}_l & l = 1, 2, \dots, d \\ (\mathbf{H}_2^T \mathbf{H}_2)^{-1} \mathbf{H}_2^T \mathbf{g}_l & l = d+1, \dots, n_1 \end{cases}$$

Denote $\mathbf{B}_1^{aug} = [\mathbf{B}_1^T, \tilde{\mathbf{B}}_{1,(q_1+1):n_1}]^T$, where $\tilde{\mathbf{B}}_{1,(q_1+1):n_1}$ is the last $n_1 - q_1$ columns of $\tilde{\mathbf{B}}_1$. Denote the marginal posterior distribution $p_{trans}(\mathbf{B}_1^T \mid \mathbf{Y}, \boldsymbol{\Theta}_{-\mathbf{B}_1, -\mathbf{B}_2})$ and $p_{trans}(\mathbf{B}_1^{aug} \mid \mathbf{Y}, \boldsymbol{\Theta}_{-\mathbf{B}_1, -\mathbf{B}_2})$ derived by the transformation of $p(\tilde{\mathbf{B}}_1 \mid \mathbf{Y}, \boldsymbol{\Theta}_{-\mathbf{B}_1, -\mathbf{B}_2})$. One has

$$\begin{aligned}
p_{trans}(\mathbf{B}_1^T \mid \mathbf{Y}, \boldsymbol{\Theta}_{-\mathbf{B}_1, -\mathbf{B}_2}) & \propto p(\mathbf{B}_1^{aug} \mid \mathbf{Y}, \boldsymbol{\Theta}_{-\mathbf{B}_1, -\mathbf{B}_2}) \\
& = p(\tilde{\mathbf{B}}_1 \mid \mathbf{Y}, \boldsymbol{\Theta}_{-\mathbf{B}_1, -\mathbf{B}_2}) \left| \frac{d\tilde{\mathbf{B}}_1}{d\mathbf{B}_1^{aug}} \right| \\
& \propto \exp \left\{ -\frac{\sum_{l=1}^{n_1} \mathbf{g}_l^T \mathbf{Q}_{1,l} \mathbf{g}_l}{2} \right\}
\end{aligned}$$

Because $\mathbf{Q}_{1,l}$ is idempotent, i.e. $\mathbf{Q}_{1,l} \mathbf{Q}_{1,l} = \mathbf{Q}_{1,l}$, the Moore–Penrose inverse of $\mathbf{Q}_{1,l}$ is $\mathbf{Q}_{1,l}$ itself. Therefore for $l = 1, \dots, d$, $\tilde{\mathbf{b}}_{1,l} \mid \mathbf{Y}, \boldsymbol{\Theta}_{-\mathbf{B}_1, -\mathbf{B}_2} \sim \mathcal{M}(\tilde{\mathbf{y}}_l, \mathbf{Q}_{1,l})$, from which the part 1 follows. Part 2 follows Lemma S1. \square

We are ready to prove Theorem 2.

Proof of Theorem 2. By Lemma S2, the posterior mean of $\tilde{\mathbf{B}}_1 \mid \mathbf{Y}, \boldsymbol{\Theta}_{-\mathbf{B}_1, -\mathbf{B}_2}$ is $\mathbf{Y}^T \mathbf{A}_F$, where $\mathbf{A}_F := [\mathbf{A}_s, \mathbf{A}_c]$. We denote the centered $\tilde{\mathbf{B}}_1$ by $\tilde{\mathbf{B}}_{1,0} = [\tilde{\mathbf{B}}_{1,Q}, \tilde{\mathbf{B}}_{1,0,c}] = \tilde{\mathbf{B}}_1 - \mathbf{Y}^T \mathbf{A}_F$, where $\tilde{\mathbf{B}}_{1,Q}$ is the first d columns of $\tilde{\mathbf{B}}_{1,0}$ and $\tilde{\mathbf{B}}_{1,0,c}$ is the next $(n_1 - d)$ columns of $\tilde{\mathbf{B}}_{1,0}$. Then the posterior mean of $\mathbf{B}_1 \mid \mathbf{Y}, \boldsymbol{\Theta}_{-\mathbf{B}_1, -\mathbf{B}_2}$ can be calculated below

$$\begin{aligned}
\hat{\mathbf{B}}_1 & = \mathbb{E}(\mathbf{B}_1 \mid \mathbf{Y}, \boldsymbol{\Theta}_{-\mathbf{B}_1, -\mathbf{B}_2}) = \mathbb{E} \left((\mathbf{H}_1^T \mathbf{H}_1)^{-1} \mathbf{H}_1^T \mathbf{A}_F \tilde{\mathbf{B}}_1^T \mid \mathbf{Y}, \boldsymbol{\Theta}_{-\mathbf{B}_1, -\mathbf{B}_2} \right) \\
& = (\mathbf{H}_1^T \mathbf{H}_1)^{-1} \mathbf{H}_1^T \mathbf{A}_F \mathbf{A}_F^T \mathbf{Y} = (\mathbf{H}_1^T \mathbf{H}_1)^{-1} \mathbf{H}_1^T \mathbf{Y}
\end{aligned}$$

Note $\mathbf{B}_1 = (\mathbf{H}_1^T \mathbf{H}_1)^{-1} \mathbf{H}_1^T \mathbf{A}_F \tilde{\mathbf{B}}_1^T$, one has

$$\mathbf{B}_1 - \hat{\mathbf{B}}_1 = (\mathbf{H}_1^T \mathbf{H}_1)^{-1} \mathbf{H}_1^T \mathbf{A}_F (\tilde{\mathbf{B}}_{1,0})^T = (\mathbf{H}_1^T \mathbf{H}_1)^{-1} \mathbf{H}_1^T (\mathbf{A}_s (\tilde{\mathbf{B}}_{1,Q})^T + \mathbf{A}_c (\tilde{\mathbf{B}}_{1,0,c})^T)$$

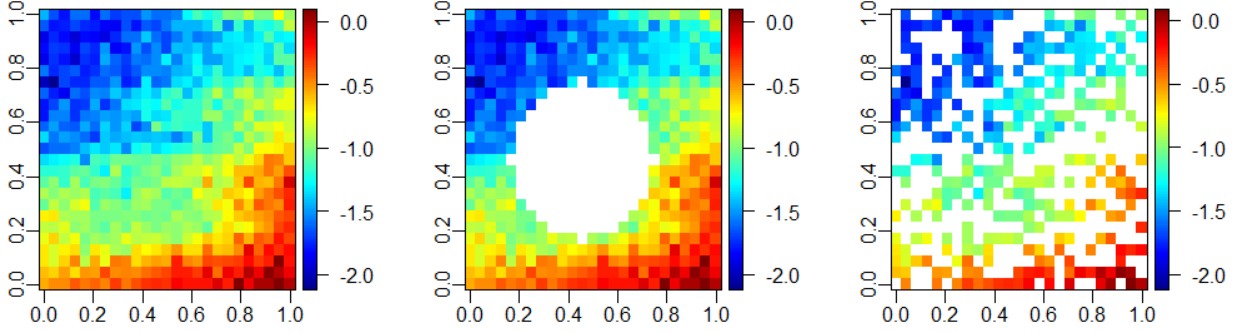


Figure S1: The simulated data with full observations, disk missing pattern and missing-at-random pattern with 50% of the missing values are graphed in the left, middle and right panels, respectively.

where by Lemma S2, $\tilde{\mathbf{B}}_{1,Q}$ is an $n_2 \times d$ matrix with the l th column independently sampled from $\mathcal{N}(\mathbf{0}, \mathbf{Q}_{1,l})$ for $l = 1, \dots, d$. For the distribution of $\mathbf{A}_c \tilde{\mathbf{B}}_{1,0,c}^T$, using part 1 of Lemma S2, we have

$$\begin{aligned} & p(\mathbf{A}_c \tilde{\mathbf{B}}_{1,0,c}^T | \mathbf{Y}, \boldsymbol{\Theta}_{-B_1, -B_2}) \\ & \propto \exp \left\{ \frac{1}{2\sigma_0^2} \text{tr} \left(\mathbf{A}_c \mathbf{A}_c^T \tilde{\mathbf{B}}_{1,0,c} \mathbf{P}_0 (\tilde{\mathbf{B}}_{1,0,c})^T \right) \right\} \\ & \propto \exp \left\{ -\frac{1}{2\sigma_0^2} \text{tr} \left((\mathbf{I}_{n_1} - \mathbf{A}_s \mathbf{A}_s^T) \tilde{\mathbf{B}}_{1,0,c} \mathbf{P}_0 (\tilde{\mathbf{B}}_{1,0,c})^T \right) \right\}. \end{aligned}$$

Thus we can sample marginal posterior distribution of $\mathbf{A}_c \tilde{\mathbf{B}}_{1,0,c}^T$ by $\sigma_0(\mathbf{I}_{n_1} - \mathbf{A}_s \mathbf{A}_s^T) \mathbf{Z}_{0,1} \mathbf{P}_0$, where $\mathbf{Z}_{0,1}$ is an $n_1 \times n_2$ matrix with each entry independently sampled from standard normal distribution. The results soon follow. \square

S2 Additional results of simulated studies in Section 5

We provide additional results for the simulated studies in Example 3 in Figure S1 and Figure S2. We graph the simulated data set with full observations, disk missing pattern and missing-at-random pattern with 50% of the missing values in Figure S1. Posterior samples of the logarithm of the inverse range parameter of factor loading matrix, the nugget parameter and the inverse range parameter of the factors are graphed from the upper to lower panels in Figure S2, respectively. The posterior samples of parameters in the exact GP model and GOLF processes are similar to each other.

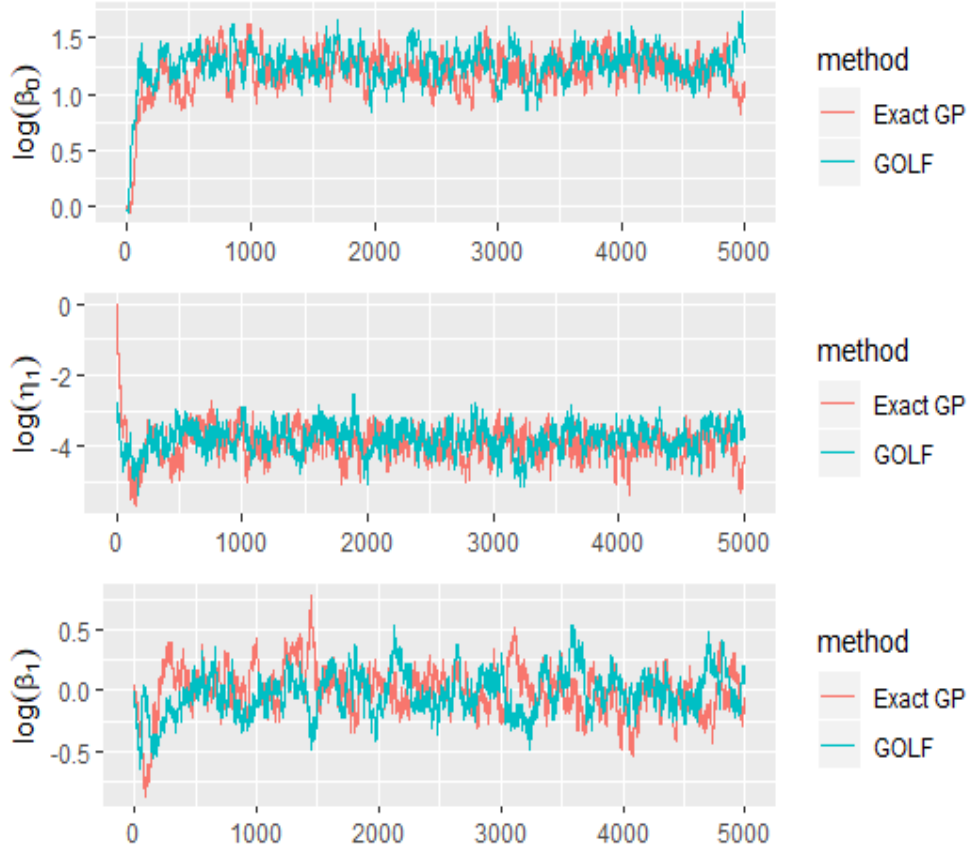


Figure S2: Trace plots of posterior samples of parameters in the exact GP model and GOLF processes for the simulated data in figure S1.

S3 Additional results for real applications in Section 6.1

In this section, we include additional results for GOLF processes predicting the missing values of the temperature data set discussed in Heaton et al. (2019). We show the details of 5 different configurations of GOLF processes, where the result reported in the main body of the article is the configuration 1. For all the configurations, the proportion of the burn-in samples is 20%. We use the normal distribution centered on the previous values as the proposal distribution of the logarithm of the inverse range parameters and logarithm of the nugget parameters. For the logarithm of the inverse range parameters of the factor loading matrix, the standard deviation of the proposal distribution is $40/n_1$. For the logarithm of the inverse range parameters and the nugget parameters of the factor processes, the standard deviation of the posterior distribution is set to be $40/n_2$.

The details of 5 configurations are given in Table S1. The predictive RMSE, $P_{CI}(95\%)$ and $L_{CI}(95\%)$ of the 5 configurations are given in Table S2. The predictive RMSE is similar for all 5 configurations. Increasing the posterior sample size seems to slightly increase the proportion of the samples contained in the 95% predictive interval.

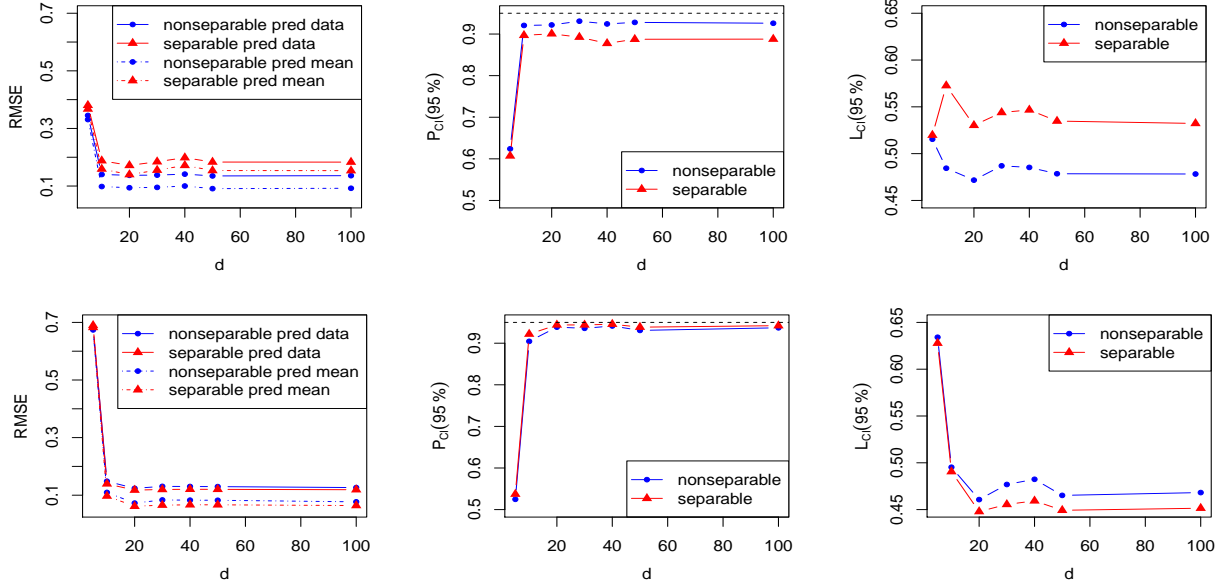


Figure S3: The predictive performance of GOLF process with $d = 5, 10, 20, 30, 40, 50$ and 100 factors for Example 4, when the true number of factor is $d_{real} = 100$ in generating the data. The nonseparable kernel with distinct kernel parameters is assumed to generate the data in the first row of panels, and the separable kernel with the same kernel parameter of each factor process is used for simulation in the second row of panels. The blue curves and red curves denote the performance by the GOLF processes with the different kernel parameters and the same kernel parameter, respectively. In the left panels, the solid curves denote the RMSE for predicting the (noisy) observations, and the dashed curve denotes the RMSE for predicting the mean of the observations. The proportions of observations covered in the 95% predictive interval and the average length of the predictive interval are graphed in the middle and right panels, respectively.

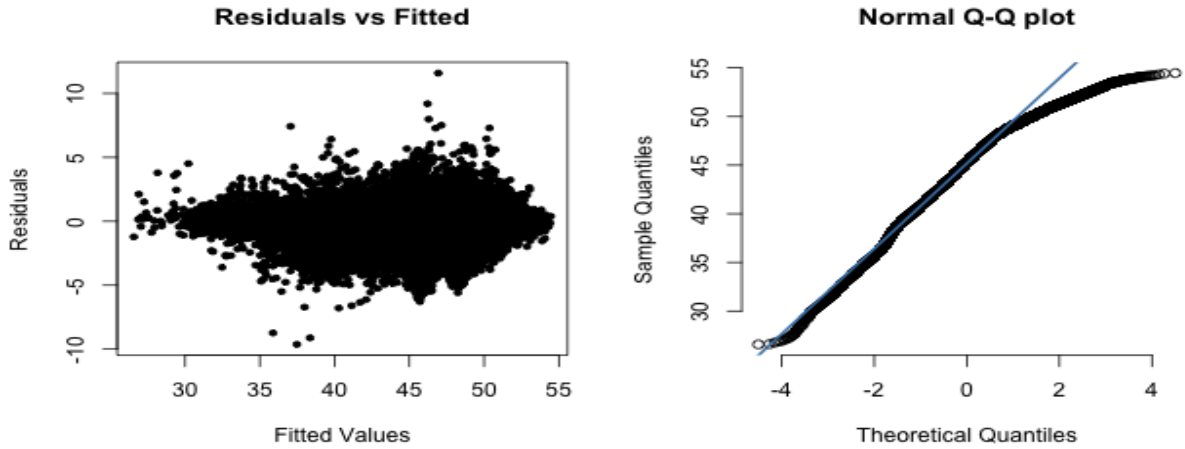


Figure S4: Diagnostic plots of the GOLF processes for the data set in Heaton et al. (2019).

	sample size	system	initial $Y_{v,i}^*$	initial $\log(\beta_0)$	initial $\log(\beta_l)$
Conf. 1	6000	Mac	mean at each latitude	3	0
Conf. 2	6000	Win	mean at each latitude	3	0
Conf. 3	40000	Mac	mean at each latitude	3	0
Conf. 4	40000	Mac	overall mean + noise	3	0
Conf. 5	40000	Mac	mean at each latitude	Unif[-1,1]	Unif[-1,1]

Table S1: Detailed settings of 5 different configurations of GOLF processes for the data set in Heaton et al. (2019). The number of samples and the computing system are shown in the second column and third column, respectively. The choice of the initial values of the missing data is given in the fourth column, using either the mean of the observations at each latitude or overall mean of the observations with a small random Gaussian noise (with standard deviation being 0.1 times of the standard deviation of the observations). The initial values of the logarithm of the inverse range parameters are either chosen to be a fixed value or randomly sampled from the uniform distribution, shown in columns 5-6.

Methods	RMSE	$P_{CI}(95\%)$	$L_{CI}(95\%)$
Configuration 1	1.46	0.92	4.95
Configuration 2	1.50	0.91	4.92
Configuration 3	1.44	0.94	7.70
Configuration 4	1.48	0.94	7.75
Configuration 5	1.51	0.93	5.16

Table S2: Predictive performance of 5 different implementations for the data set in Heaton et al. (2019).

The fitted values from the GOLF processes in configuration 1 against the residuals and the normal Q-Q plot are graphed in the left panel and the right panel in Figure S4, respectively. The Q-Q plot indicates the fitted values are slightly left-skewed and slightly under-dispersed.